Identification of an altered matrix signature in kidney ageing and disease

*Michael J Randles[1#], *Franziska Lausecker[1], Qingyang Kong[2], Hani Suleiman[3], Graeme Reid[4], Maria Kolatsi-Joannou[5], Bernard Davenport[1], Pinyuan Tian[1], Sara Falcone[6], Paul Potter[7], Tom Van Agtmael[8], Jill T Norman[2], David A Long[5], Martin J Humphries[1], Jeffrey H Miner[3] and Rachel Lennon[1,9]

1.Wellcome Centre for Cell-Matrix Research, Division of Cell-Matrix Biology and Regenerative Medicine, School of Biological Sciences, Faculty of Biology Medicine and Health, The University of Manchester, Manchester Academic Health Science Centre, Manchester, UK. 2. Department of Renal Medicine, University College London, London, UK. 3. Renal Division, Washington University School of Medicine, Saint Louis, MO, USA. 4. Department of Histopathology, Manchester Royal Infirmary, Manchester University Hospitals NHS Foundation Trust, Manchester Academic Health Science Centre, Manchester, UK. 5. Developmental Biology and Cancer Programme, UCL Great Ormond Institute of Child Health, London, UK. 6. Centre for Cellular and Molecular Physiology, University of Oxford, Oxford, UK. 7. Department Biological and Medical Sciences, Faculty of Health and Life Sciences, Oxford Brookes University, UK. 8. Institute of Cardiovascular and Medical Sciences, University of Glasgow, University Avenue, Glasgow G12 8QQ, United Kingdom. 9. Department of Paediatric Nephrology, Royal Manchester Children's Hospital, Manchester University Hospitals NHS Foundation Trust, Manchester Academic Health Science Centre, Manchester, UK.

**These authors contributed equally to this work.*
#Present address: Faculty of Medicine, Dentistry and Life Sciences, Chester Medical School, University of Chester, Chester, UK.

Running title: Matrix signature in ageing and disease

Word count: Abstract: 248 Text: 3414

Corresponding author:
Rachel Lennon: Wellcome Centre for Cell-Matrix Research, Michael Smith Building, University of Manchester, M13 9PT, UK.
Email: Rachel.Lennon@manchester.ac.uk

Keywords:
Extracellular matrix, basement membrane, mass spectrometry, proteomics, glomerulus, tubulointerstitium, fibrosis, matrix signature, type IV collagen, type VI collagen, nephronectin.

Abstract

Background: Accumulation of extracellular matrix in organs and tissues is a feature of both ageing and disease. In the kidney, glomerulosclerosis and tubulointerstitial fibrosis accompany the decline in organ function, which is irretrievable with current therapies leading to inevitable kidney failure. Whilst histological and ultrastructural patterns of excess matrix form the basis of human disease classifications, the comprehensive molecular resolution of abnormal matrix is lacking. **Methods:** Using mass spectrometry-based proteomics we resolved matrix composition over age in mouse models of kidney disease. We compared the changes in mice with a global characterization of human kidney matrix during ageing and to existing kidney disease datasets to identify common molecular features. **Results:** We found that ultrastructural changes in basement membranes are associated with altered cell adhesion and metabolic processes and with distinct matrix proteomes during ageing and kidney disease progression in mice. Within the altered matrix, we observed a reduction in basement membrane components (laminins, type IV collagen, type XVIII collagen) and a corresponding increase in interstitial matrix proteins (collagens I, III, VI, XV, fibrinogens and nephronectin) and this pattern was also seen in human kidney ageing. Indeed, this signature of matrix proteins was consistently modulated across all age and disease comparisons and the increase in interstitial matrix was also observed in human kidney disease datasets. **Conclusions:** This study provides deep molecular resolution of matrix accumulation in kidney ageing and disease and identifies a common signature of proteins that provides insight into mechanisms of response to kidney injury and repair.

Introduction

Extracellular matrix (ECM) is organized as basement membranes, which support continuous layers of cells, or as looser interstitial matrix (1). In addition to providing a scaffold ECM directs organ shape and sequesters growth factors and enzymes for controlled outside-in signalling (2). This extracellular environment is complex and dynamic with over 1000 matrisome proteins annotated (3). Matrix synthesis and turnover requires tight regulation for the maintenance of organ function, and matrix accumulation is associated with a wide spectrum of human disease. 45% of deaths in the Western world have been associated with organ fibrosis (4). Thus, understanding the drivers of matrix accumulation is key to identifying strategies to prolong organ survival.

Excess matrix is seen across a wide spectrum of pathology and is incorporated into the histological and ultrastructural descriptions of many diseases (5). In the kidney, glomerulosclerosis is feature of ageing and glomerular disease (6) and tubulointerstitial fibrosis is seen with both primary tubular disease and as a consequence of glomerular disease (7, 8), yet the comprehensive molecular definition of altered matrix is limited. The use of proteomics to define global protein composition has improved the resolution of matrix complexity and this includes the human glomerular matrisome, which contains over 140 structural and regulatory components (9, 10). Proteomic studies in kidney disease have also revealed changes in matrix composition (11, 12) but these have been limited by sample volume and have not utilized matrix enrichment strategies, which improve resolution (13).

Along the nephron there is distinct matrix composition within basement membranes and interstitial matrices (14). Basement membranes underly parietal epithelial cells, separate endothelial cells from overlying podocytes, provide a scaffold for tubular epithelial cells and form an integral component of blood vessel walls in the kidney. Interstitial matrices include the mesangial matrix and the loose tubulointerstitial matrix. The glomerular and tubular segments of the nephron have distinct functions and their differential matrix composition is likely to reflect their underlying functions including filtration and reabsorption. One example of structure supporting function is the triple helix of type IV collagen protomers, which may resist mechanical load (15) and could explain the distinct localisation of collagen IV isoforms along the nephron.

Here we performed deep proteomic profiling to define global changes in kidney matrix and to identify common components and pathways. In mouse models of genetic defects in collagen IV we found distinct matrix structural abnormalities associated with altered cell adhesion and

metabolic processes and a signature of abnormal matrix composition. In young and aged human kidneys and existing kidney disease datasets we identified a similar signature of altered matrix. Broadly we observed a reduction in basement membrane components and an increase in interstitial matrix proteins in both mouse models and human tissue.

Methods

Antibodies: Primary antibodies were diluted in a blocking buffer (1% donkey serum, 2% BSA, 0.1% Triton-X 100 in PBS). Primary antibodies used were against type VI collagen (ab6588, abcam) at 1/100 dilution and 1/500 dilution for STORM imaging, type IV collagen chains: α1, α2, α3, α4, α5 and α6 (7070, 7071, 7076, 7073, 7077, and 7074, respectively, Chondrex, Washington, USA) at 1/200 dilution, type I collagen (OARAO2579, Gentaur, Kapenhout, Belgium) at 1/100 dilution, podocin ab50339 (Abcam) at 1/400 dilution, fibulin-1 (sc-25281; Santa Cruz Biotechnology, Dallas, USA) at 1/100 dilution, nidogen/entactin antibody (MAB1946, ELM1, Merck, Germany) at 1/100 dilution, laminin beta 2 (ab210956, abcam) at 1/100 dilution, Tinag (ab67614, abcam) at 1/100 dilution, integrin beta1 (BD Pharmigen, clone 9EG7) at 1/500. Secondary antibodies conjugated to Alexa Fluor 488 or 594 (Life Technologies) were used for immunofluorescence.

Mice: We used *Col4a1*$^{+/SVC}$ mice, which carry a point mutation causing an amino acid substitution (G1064D) (16). These mice were on a BL6/C57 background, we used littermate controls, male mice for phenotypic consistency and n=3 mice from each group for proteomic analysis. *Col4a3*$^{-/-}$ mice were generated as described (17). In brief, the first three exons of the COOH-terminal (NC1) domain of collagen-α3(IV) chain were deleted, causing absence of collagen-α3(IV) protein. *Col4a5*$^{-/-}$ mice were obtained from the International Mouse Phenotyping Consortium (18). The line was generated by deletion of the critical exon 36 resulting in the absence of the collagen-α5(IV) protein with the published allele map (19). *Col4a3*$^{-/-}$ and *Col4a5*$^{-/-}$ mice were on a BL6/C57 background, we used littermate controls, male mice for phenotypic consistency and we used n=5 mice from each group for proteomic analysis. All experiments were performed in compliance with the ASPA regulations of the UK Home Office.

Glomerular isolation from mice Cortical tissue was dissected from frozen-thawed, kidney placed in a glass dish and cut into small pieces (≤1mm^3) as previously (9). Tissue pieces were washed three times with PBS. Tissue pieces were transferred onto a 100 µm cell strainer (Falcon) and mechanically disintegrated. PBS was added and flow through was collected. The resulting tissue solution was filtered through a 70 µm cell strainer (Falcon). Glomeruli were

caught on the 70 µm cell strainer. The cell strainer was inverted and caught glomeruli were washed off the sieve and collected in a container.

Human kidney: Human kidneys (n=6) anatomically unsuitable for transplantation and with no recorded comorbidities, were collected under ethical approval [Regional Ethics Committee approval 05/Q0508/6 (University College London) and 06/Q1406/38 (Manchester)]. Samples were grouped into young (15, 29, 37 years) and aged (61, 67, 69 years) with n=3 per group. 5 of the 6 kidneys were from male donors and the sex of the 67 year old kidney was not recorded. Kidney biopsy sections from a male patient presenting at age 14 years with chronic kidney disease stage 3 due to autosomal recessive (*COL4A3*) Alport syndrome, and control kidney tissue (non-affected tissue of tumor nephrectomy) were also used with ethical approval 06/Q1406/38 (Manchester).

Glomerular and tubulointerstitial isolation from human kidney: Cortical tissue (2g) was dissected from frozen-thawed kidney placed in a glass dish and cut into small pieces (≤1mm^3) as previously (9). Graded sieves 250µm, 150µm and 106µm were assembled with the 250µm sieve at the top and placed on a collection container. Tissue pieces were transferred onto the largest sieve in 5ml ice-cold PBS (without calcium and magnesium). The plunger from a 10ml syringe was used to press the sample through the sieves. Fragments were washed through the sieves with 60-100ml of ice-cold PBS. Glomeruli were retained on 150µm and 106µm sieves and were collected by inverting the sieves and washing with 20ml ice-cold PBS. Cortical tubulointerstitial (TI) fragments were retrieved from the collection container. The glomeruli and TI samples were centrifuged at 3,000xg for 3 minutes at 4°C then washed 3 times by centrifugation and resuspension in 10ml ice-cold PBS. After the final wash, samples were resuspended in 5ml PBS and aliquoted into five 1ml aliquots. One aliquot from each sample was viewed under a light microscope to confirm the separation of glomeruli and TI tissue. One aliquot was frozen at -20°C for ECM enrichment and the remainder stored at - 80°C.

Matrix enrichment: Samples stored at -20°C were defrosted at room temperature, homogenized using a 21G needle and 2ml syringe and centrifuged at 14,000xg for 5 minutes at room temperature. Ice-cold buffer solution 1 (500µl; 10mM Tris, 150mM sodium chloride, 25mM EDTA, 1% (v/v) Triton X-100, 25µg/ml leupeptin, 25µg/ml aprotinin, 0.5mM 4-(2-Aminoethyl)benzenesulfonyl fluoride hydrochloride (AEBSF)) was added to the pellet and samples incubated on ice for 1 hour. Samples were centrifuged at 14,000xg for 10 minutes at 4°C, the supernatant was collected and mixed with 125µl recovery buffer (15% (w/v) SDS, 100mM 1,4-dithiothreitol (DTT), 200mM Tris, 30% (v/v) glycerol), 0.01% Bromophenol blue).

This sample was designated soluble fraction 1 (most of the cellular compartment) and stored at -80°C. The pellet was resuspended in 500µl ice-cold buffer solution 2 (20mM NH4OH, 0.5% (v/v) Triton X-100) and incubated on ice for 1 hour. Samples were centrifuged at 14,000 x g for 10 minutes at 4°C, the supernatant collected and designated soluble fraction 2. The pellet was resuspended in 500µl PBS with DNase I (25µg/ml) and incubated for 30 minutes at room temperature. Samples were centrifuged at 14,000xg for 10 minutes at 4°C, the supernatant collected as soluble fraction 3. The final pellet was resuspended in a sample buffer and incubated for 10 minutes at 95°C to generate the ECM-enriched fraction.

Mass spectrometry data acquisition: Following SDS–PAGE, gel lanes were sliced and subjected to in-gel digestion with trypsin (20) with modifications (21). Peptide samples were analyzed by liquid chromatography (LC)-tandem MS using a nanoACQUITY UltraPerformance LC system (Waters) coupled online to an LTQ Velos mass spectrometer (Thermo Fisher Scientific) or using an UltiMate 3000 Rapid Separation LC system (Thermo Fisher Scientific) coupled online to an Orbitrap Elite mass spectrometer (Thermo Fisher Scientific). Peptides were concentrated and desalted on a Symmetry C18 preparative column (20 mm × 180 µm, 5-µm particle size; Waters) and separated on a bridged ethyl hybrid C18 analytical column (250 mm × 75 µm, 1.7-µm particle size; Waters) using a 45-min linear gradient from 1% to 25% or 8%–33% (v/v) acetonitrile in 0.1% (v/v) formic acid at a flow rate of 200 nl min−1. Peptides were selected for fragmentation automatically by data-dependent analysis.

Mass spectrometry identifications: Tandem mass spectra were extracted using extract_msn (Thermo Fisher Scientific) executed in Mascot Daemon (version 2.5.1; Matrix Science). Peak list files were searched against a modified version of the Uniprot mouse database (April 2016 database selected for Mus musculus) for mouse datasets, or Uniprot human database (November 2015 database selected for Homo Sapiens) for human datasets. Carbamidomethylation of cysteine was set as a fixed modification; oxidation of methionine and hydroxylation of proline and lysine were allowed as variable modifications. Only tryptic peptides were considered, with up to one missed cleavage permitted. Monoisotopic precursor mass values were used, and only doubly and triply charged precursor ions were considered. Mass tolerances for precursor and fragment ions were 5 ppm and 0.5 Da, respectively.

Mass spectrometry quantification: Relative protein abundance was calculated using peptide intensity. Orbitrap MS data were entered into Progenesis LC-MS (Non Linear Dynamics Ltd) and automatically aligned. Spectra were extracted using extract_msn executed

in Mascot Daemon (version 2.5.1; Matrix Science) and imported back into Progenesis LC-MS to acquire intensity data. Alignment of chromatograms was carried out using the automatic alignment algorithm, followed by manual validation and adjustment of the aligned chromatograms. All features were used for peptide identifications. Progenesis LC-MS created the peak list file that was exported and searched in Mascot. Protein abundance was inferred using Hi-N with the three most abundant peptides being used (22). Peptide and protein data were then exported from Progenesis LC-MS as.csv files to be analysed in Excel (Microsoft). Proteins identified by 1 unique peptide and a Mascot score indicating a <5% false discovery rate, were considered to be part of the definition of the human tubulointerstitial matrisome. The data was further filtered to include only proteins present in 2 out of 3 tubulointerstitial samples in a specific age group. Proteins identified by 3 unique peptides and a Mascot score indicating <5% false discovery rate were considered for quantitative analysis. Protein abundance was inferred from normalized peptide intensities using the 3 most abundant unique Hi-N peptides setting in Progenesis. Protein grouping was employed to resolve conflicts. Group protein abundances were compared across samples using ANOVA with post-hoc Bonferroni. To enable Gene Ontology lists with sufficiently large numbers of proteins in all comparisons, proteins with $p<0.1$ and 1.4 fold increased or decreased abundance were taken forward for further analysis.

Protein interaction network analysis: Protein interaction network analysis was performed using Cytoscape (version 3.7.2). Matrisome proteins were selected from the Matrisome Project (3) and proteins identified in at least two biological replicates were mapped onto a merged human, mouse and rat interactome. This was built from the PICKLE 2.5 (released on November 15 2019) (based on IntAct release 227/2019-11-04, BioGRID release 3.5.178, DIP release 20170205 and HPRD release 9) database merged with a matrix protein specific interactome Protein Interaction Network Analysis platform Homo sapiens network (release date, December 10, 2012), Mus musculus network (release date, December 10, 2012) and the Rattus norvegicus network (release date, December 10, 2012), the ECM interactions database MatrixDB (release date, April 20, 2012), and a literature-curated database of integrin-based adhesion–associated proteins (23). For networks where enrichment/fold change is presented, Progenesis LC-MS normalized intensity data were used. Networks were manually grouped.

Data analysis: Functional enrichment analysis was performed using DAVID (version 6.7). Keywords with fold enrichment ≥ 1.5, Bonferroni-corrected p value < 0.05, EASE score (modified Fisher's exact test) < 0.05 and at least two proteins per keyword were considered

significantly overrepresented. Enrichment maps were generated using all changed proteins detected, p<0.1-fold change at least >1.4. Enrichment maps were clustered using the clusterMaker app with MCL tuning, granularity parameter 2.5. Principal component analysis was performed using MATLAB (version R2019a; MathWorks). Hierarchically clustered heat maps were generated on the basis of uncentred Euclidean complete linkage clustering in MultiExperiment Viewer (version 4.8.1). For clustered heat maps where Z-score or fold change is presented, Progenesis LC-MS normalized intensity data were used.

Nephroseq analysis: Nephroseq v5 was used for analysis. Signature matrix proteins were searched for their fold change in gene expression in disease datasets compared to associated control samples. The following filters were applied: tissue type; glomeruli and analysis type; disease versus control analyses. Microarray data were extracted with the p-value selection: all and fold change: all. The primary data is shown in **S.Table 4. Figure 8E** shows data which met the following criteria: p-value <0.05, FC = +/- 1.5, these are highlighted in orange in **S.Table 4**. Data is shown as box and whiskers plots displaying all data points. Values below every plot indicates the number of datasets that a transcript was detected out of all analysed datasets (21 datasets). Data from the following datasets were extracted: **Berthier Lupus Glom**; analysis: Lupus Nephritis vs. Healthy Living Donor (24), **Hodgin Diabetes Mouse Glom**, analyses; Diabetic Nephropathy vs. Non-Diabetic Kidney (mouse model db/db C57BLKS), Diabetic Nephropathy vs. Non-Diabetic Kidney (Mouse Model DBA/2), Diabetic Nephropathy vs. Non-Diabetic Kidney (Mouse Model eNOS-deficient C57BLKS db/db) (25), **Hodgin FSGS Glom**, analyses; Collapsing Focal Segmental Glomerulosclerosis vs. Normal Kidney, Focal Segmental Glomerulosclerosis Vs. Normal Kidney, Minimal Change Disease vs. Normal Kidney (26), **Ju CKD Glom,** analyses; Arterial Hypertension vs. Healthy Living Donor, Diabetic Nephropathy vs. Healthy Living Donor, Focal Segmental Glomerulosclerosis vs. Healthy Living Donor, IgA Nephropathy vs. Healthy Living Donor, Lupus Nephritis vs. Healthy Living Donor, Minimal Change Disease vs. Healthy Living Donor, Membranous Glomerulonephropathy vs. Healthy Living Donor, Tumor Nephrectomy vs. Healthy Living Donor, Thin Basement Membrane Disease vs. Healthy Living Donor, Vasculitis vs. Healthy Living Donor , **Neusser Hypertension Glom,** analysis; Nephrosclerosis vs. Tumor Nephrectomy (27), **Peterson Lupus Glom**, analysis; Lupus Nephritis vs. Normal Kidney (28), **Reich IgAN Glom**, analysis; IgA Nephropathy vs. Healthy Living Donor (29) **Woroniecka Diabetes Glom**, analysis; Diabetic Nephropathy vs. Healthy Living Donor (30).

Electron microscopy: Samples were prepared as previously (31). Briefly, mouse kidneys were harvested and immediately cut into 1 mm^2 pieces and fixed in 2.5% glutaraldehyde, 4%

paraformaldehyde and 0.1M HEPES pH7.4. Samples were stained in 1% osmium tetroxide, 1.5% potassium ferrocyanide in 0.1M cacodylate buffer, followed by 1% thiocarbohydrazide. Samples were washed and stained further in 1% osmium tetroxide and incubated in 1% uranyl acetate overnight. Samples were incubated in lead aspartate pH5.5 for 1h at 60°C, dehydrated and finally embedded in TAAB 812 hard resin. Samples were mounted onto an aluminium cryo pin. Block surfaces were trimmed using a glass knife or diamond trimming tool. To create a conductive surface, a gold coating was applied to the specimen. The samples were analysed using a Quanta 250 FEG (FEI Company) + Gatan 3view system. The analysed *Col4a1*$^{+/SVC}$ received treatment with 4-Sodium phenyl butyric acid as described before which did not affect the kidney phenotype (32) Kidney samples for transmission electron microscopy were fixed as for serial block face-scanning electron microscopy. 70-80nm thick sections were prepared and examined using a FEI Tecnai 12G2 Biotwin transmission electron microscope. Foot process width, GBM thickness and Bowman's capsule basement membrane thickness were measured using ImageJ (Version 2.0.0-rc-68/1.52e). Foot process width was measured at the basal side of podocytes from 10 different fields of view in the glomerulus. Measurements were taken from one glomerulus per mouse genotype. GBM thickness was measured radially from the endothelial side of the electron-dense GBM to the basal membrane of podocyte foot processes. Bowman's capsule thickness was measured radially in different sections of the acquired serial block face-scanning electron microscopy stack from one glomerulus.

Light microscopy: Formaldehyde-fixed, paraffin-embedded kidney sections were used for immunofluorescence. Images were acquired using a Zeiss Axioimager.D2 upright microscope using a 20x / 0.50 EC Plan-neofluar and captured using a Coolsnap HQ2 camera (Photometrics) through Micromanager software v1.4.23. Images of stained cryosections were acquired using a Zeiss AxioObserver Z1 wide-field microscope equipped with a 40x / EC Plan-neofluar 1.3 Oil objective and an Axiocam MRm camera, controlled by Zeiss Axiovision software. Specific band pass filter sets for DAPI, FITC and Texas red were used to prevent bleed through from one channel to the next. Images were processed and analysed using ImageJ (Version 1.51j8 and version 2.0.0-rc-68/1.52e). Total positive antibody fluorescence was measured in glomeruli and the TI separately and normalized to the total background in the same area to generate corrected total fluorescence. Background was subtracted using a rolling ball algorithm in ImageJ in the shown immunofluorescent images in **Figure 3** and **Figure 8**.

Tissue preparation and staining for STORM imaging: Tissue was fixed and stained as described previously (33, 34). In brief, kidneys were fixed in 4% paraformaldehyde (PFA) in

PBS. Samples were washed in PBS incubated in a cryoprotectant solution of 2.3M sucrose plus 10% polyvinylpyrrolidone (PVP) in 0.1M piperazine-N, N'-bis (PIPES) at pH = 7.2 at 4°C overnight. Tissue pieces were mounted on a metal sectioning pin and frozen in liquid nitrogen. Frozen tissue was sectioned using an EM-FC6 ultracryomicrotome (Leica) and collected on carbon-coated coverslips. Sections were fixed in 4% PFA for 20 minutes, washed with PBS and PFA was quenched using 50mM glycine in PBS. For immunofluorescence, sections were blocked in 2% BSA in PBS overnight followed by another overnight incubation of primary antibodies diluted in 2% BSA in PBS. After washing, sections were incubated with secondary antibodies diluted in 2% BSA in PBS for 2 hours at room temperature. Secondary antibodies for Direct-STORM were purchased from Jackson ImmunoResearch Laboratories and custom conjugated to Andy Fluor-488, -Cy3 or Cy5 reporter dyes as described previously (34). Sections were washed again in PBS and postfixed in 3% PFA plus 0.05% glutaraldehyde in PBS. After a final washing series, samples were imaged by Nikon N-STORM according to the manufacturer's instructions as described (34).

Histology: Paraffin embedded mouse tissue sections were stained using a Shandon Linistain GLX stainer (Thermo Fisher) for hematoxylin and eosin. Samples were mounted using Histokitt solution (Roth). For Picro Sirius Red staining, paraffin-embedded tissue sections were dewaxed using a Leica ST5010 autostainer. Tissue sections were stained by incubation of slides in picro-sirius red solution [(0.5g Sirius Red (Sigma) and 500ml of saturated aqueous solution of picric acid (Sigma)] for one hour. Slides were washed in acidified water. Slides were dehydrated and mounted using Histokitt solution (Roth). Images were collected on an Olympus BX63 upright microscope using a 60x / 1.42 PlanApo N objective and captured and white-balanced using a DP80 camera (Olympus) in colour/polarised light mode through CellSens Dimension v1.16 (Olympus). For TriPAS staining paraffin sections were dewaxed and placed into 1% periodic acid for 10 minutes, and washed with tap and distilled water. Nuclei were stained with Gills No.2 haematoxylin for 1.5 minutes and washed in tepid tap water. Sections were stained in 2% orange G dissolved in 100 ml of 5% phosphotungistic acid for 1 minute. Sections were washed, dehydrated and coverslipped. For human and mouse sections, a specialist kidney pathologist performed percentage glomerulosclerosis analysis and percentage interstitial fibrosis and tubular atrophy (IFTA) scoring on the TriPAS-stained tissue sections.

Urinary albumin and creatinine analysis: Spot urine was collected at the same time of the day for each group of mice. Urinary albumin was measured using a mouse albumin ELISA kit

(E99-134, Bethyl Laboratories). Creatinine was measured using a creatinine ELISA assay according to Manufacturer's instructions (KGE005, R&D systems).

Data sharing information: The proteomics data were deposited in the ProteomeXchange Consortium (35) via the PRoteomics IDEntifications database (PRIDE) partner repository with the dataset identifier PXD022363 "Col4a1 mouse glomerular datasets", PXD022392 "Col4a3 mouse glomerular datasets", PXD022227 "Col4a5 mouse glomerular extracellular matrix and cellular fraction", PXD022219 "Human kidney proteomics, glomerular and tubular cellular and matrix fractions".

Statistical analysis: Data presented as bar charts (mean±SEM) or box-and-whisker plots and were analyzed using GraphPad Prism (version 7, GraphPad Software, La Jolla, CA, USA). Data were analyzed by Shapiro-Wilk test for normality and analyzed by Kruskal-Wallis test or ANOVA with post-hoc Bonferroni correction or t-test as appropriate. Statistical significance was accepted at $p < 0.05$. Principal component analysis was performed in MATLAB. Unsupervised hierarchical clustering was performed in T4MeV using a Euclidean distance-based complete-linkage matrix.

Results

Structural and compositional change in matrix

Type IV collagen is an essential component of basement membranes (BM) in the kidney and exists as three networks comprised of α1.α1.α2(IV), α3.α4.α5(IV) and α5.α5.α6(IV) heterotrimers. We confirmed the glomerular localization of these three networks with α1.α1.α2(IV) in the mesangium, GBM and Bowman's capsule; α3.α4.α5(IV) in the GBM; and α5.α5.α6(IV) in Bowman's capsule (**S.Figure 1**). To understand the impact of glomerular disease on matrix we investigated three mouse models with defects in the different collagen IV heterotrimers. Firstly *Col4a1*$^{+/SVC}$ mice, which harbor a glycine to aspartic acid variant (G1064D) and have phenotypic overlap with human *COL4A1* variants, including defects in Bowman's capsule, kidney cysts and tubular dysfunction (32, 36). Secondly *Col4a3*$^{-/-}$ mice (autosomal recessive Alport syndrome), which have progressive glomerular disease associated with GBM defects (17), and thirdly a new *Col4a5*$^{-/-}$ model of X-linked Alport syndrome. We characterized the *Col4a5*$^{-/-}$ mice and demonstrated abnormal GBM thickness, podocyte effacement and progressive albuminuria **(S.Figure 2)**. To investigate the impact of *Col4a* defects on matrix ultrastructure, we performed serial block-face scanning electron microscopy of young (6-8 weeks), adult (16-18 weeks) and aged (28 weeks) mice (**Figure 1A-D and S. Videos 1-4**). GBM thickness was similar to wild type in adult *Col4a1*$^{+/svc}$ mice but

thickened in adult *Col4a3*$^{-/-}$ and *Col4a5*$^{-/-}$mice. Podocyte foot process width was preserved in *Col4a1*$^{+/svc}$ mice but increased over age with *Col4a3*$^{-/-}$ and *Col4a5*$^{-/-}$ mice. Bowman's capsule BM thickness was increased in adult *Col4a3*$^{-/-}$ mice compared to adult wild type and *Col4a5*$^{-/-}$ mice and markedly thickened in aged *Col4a3*$^{-/-}$ mice (**S. Video 3**). Adult *Col4a1*$^{+/svc}$ mice had normal thickness of Bowman's capsule BM, but there was infiltration of parietal epithelial cells. Given these structural changes in the matrix, we analyzed matrix composition using mass spectrometry-based proteomics. To interrogate changes that precede, and also coincide with ultrastructural changes, we analyzed glomerular proteomes in young and adult mice. We isolated glomeruli and separated cellular and matrix fractions from n=3 (*Col4a1*$^{+/svc}$), n=5 (*Col4a3*$^{-/-}$) and n=5 (*Col4a5*$^{-/-}$) mice and their respective littermate controls as previously described (9). Proteins were taken forward if identified by 3 unique peptides with a Mascot score indicating a <5% false discovery rate. Gene Ontology (GO) enrichment analysis highlighted increases in cell matrix and cell adhesion ontologies and a reduction in mitochondrial and metabolic components in all three *Col4a* models compared to controls (**Figure 1E**). Equivalent analyses of individual *Col4a* datasets highlighted similar cellular pathways **(S.Figure 3A)** and principal component analysis (PCA) demonstrated model and age segregation (**Figure 2A**). Taken together these findings highlight both structural and compositional changes in matrix in models of glomerular disease.

Evolution of altered matrix in ageing and disease

To explore the altered glomerular matrix we focused on the matrix-enriched fractions where 707 (*Col4a1*$^{+/svc}$), 334 (*Col4a3-/-*) and 600 (*Col4a5*$^{-/-}$) proteins were detected. Volcano plots revealed age and genotype specific changes in protein identifications **(Figure 2B-E)**. In keeping with predictions based on genotype, collagen-α1(IV) and collagen-α2(IV) were reduced in *Col4a1*$^{+/svc}$ glomeruli but moderately increased in both *Col4a3*$^{-/-}$ and *Col4a5*$^{-/-}$ glomeruli **(Figure 2F and S.Figure 4A)**. In addition, both collagen α3.α4.α5(IV) and laminin 521 were reduced in *Col4a3*$^{-/-}$ and *Col4a5*$^{-/-}$ in contrast to *Col4a1*$^{+/svc}$ glomeruli **(Figure 2F and S.Figure 4A)** and immunofluorescence confirmed reduced levels of collagen-α3(IV) and collagen-α4(IV) in *Col4a5*$^{-/-}$ mice (**S.Figure 4B**). Although ultrastructure was preserved in young Alport mice (**Figure 1**), we observed altered matrix composition (**Figure 2B,D and S.Figure 5A and 6A**) with a broad reduction in BM components and an increase in interstitial matrix. This pattern was exaggerated in the older mice (**Figure 2C,E and S.Figure 5B and 6B**). Although less pronounced there were also changes during ageing in wild type mice, with reduced collagen IV and increased collagen VI (**S.Figure 3B**). We performed immunofluorescence on *Col4a5*$^{-/-}$ kidney sections and also observed increased collagen VI, collagen I and reduced laminin-β2 and Tinag (**Figure 3A,B**). For greater spatial resolution we

used stochastic optical reconstruction microscopy (STORM) to determine the localization of increased collagen VI. Control heterozygous *Col4a3*$^{+/-}$ mice have normal kidney function (37) and we detected regular integrin β1 fluorescence and no GBM collagen VI. However, in *Col4a3*$^{-/-}$ mice we detected collagen VI in expanded regions of GBM (**Figure 3C**). Overall we found altered matrix composition prior to overt ultrastructural changes and these changes increased in ageing and disease progression.

Increased cell-matrix adhesion in disease

To connect the altered matrix with cell-matrix adhesion, we used the consensus adhesome (38) to select integrin adhesion complex components from all three disease model datasets (**Figure 4**)**.** The consensus adhesome is centred around four dominant signalling hubs: ILK-PINCH-kindlin; FAK-paxillin; talin-vinculin and α-actinin-zyxin-VASP. Examining proteins detected in cellular and matrix fractions across these hubs, we found a global increase in abundance of integrin adhesion components and their respective ligands. In particular we found parallel increases in the collagen binding integrins (α1β1, α2β1) with collagen VI, collagen I and collagen III in addition to the parallel increase in α8β1 and its ligand nephronectin. The observed global increase in adhesion components may reflect greater receptor-ligand interaction associated with podocyte effacement.

Altered glomerular matrix in human kidney ageing

Having observed altered matrix in ageing and disease in mice, we examined human tissue. Glomerulosclerosis, tubular atrophy and interstitial fibrosis are observed in human ageing (45). Therefore, we investigated changes in matrix over age using unused human donor kidneys. Sections of young (15, 29, 37 years) and older (61, 67, 69 years) human kidneys were assessed blindly by a kidney pathologist who reported occasional focal glomerular and interstitial damage consistent with age. From these kidneys, glomeruli were isolated, subjected to matrix fractionation and analyzed by mass spectrometry. PCA of matrisome proteins showed good separation by age (**Figure 5A**) and GO enrichment analysis of all detected proteins highlighted matrix and cell-matrix ontologies **(S.Figure 7A)**. Volcano plots and hierarchical clustering highlighted glomerular matrix proteins changing with age (**Figure 5B,C**). There was a skewed distribution with a greater number of increased abundance proteins in aged samples, including collagen VI and TIMP3 (**Figure 5B**). Fewer proteins were enriched in younger glomeruli including filaggrin-2, ECM1 and agrin. Protein-protein network mapping highlighted a reduction in BM components, including laminins and collagen IV, and an increase in interstitial matrix proteins (**Figure 5D**). Overall these findings highlight altered

composition of matrix during human glomerular ageing with similarity to ageing and disease in mice.

Defining the human tubulointerstitial matrisome

Together with altered glomerular matrix in kidney ageing and disease, there are changes in the tubulointerstitium (8) Matrix in this kidney compartment has received far less research attention and so we first defined the human tubulointerstitial (TI) matrisome**.** We isolated TI matrix from n=6 human kidneys (as above) for analysis by mass spectrometry. We included proteins identified by 1 unique peptide and a Mascot score indicating a <5% false discovery rate and present in 2 out of 3 samples in each age group. We robustly identified 141 proteins (**S.Table 2**) **(S.Figure 8A,B)** and 90% of all the components were also found in the glomerular matrix from this study and our previous investigation (9) Comparison of human glomerular and TI matrix revealed distinct proteomes **(S.Figure 8C)**. Collagen-α3.α4.α5(IV) was abundant in the glomerular matrix, but also detected in the tubulointerstitium, which we validated by immunofluorescence (**S.Figure 9A**). We screened the Human Protein Atlas (39) to confirm localization of 67 components in the tubulointerstitium and 80 in both glomerular and TI compartments (**S.Figure 9B,C**). Combining the glomerular and TI datasets allowed us to define the combined human kidney matrisome, dominated by proteoglycans, collagens and a wide variety of matrix regulators and secreted factors (**S.Figure 10**). Together these data highlight the complexity of the TI matrix and key compositional differences with the adjacent glomerular compartment.

Altered tubulointerstitial matrix in human kidney ageing

Having defined the human TI matrisome, we compared TI matrices from young (15, 29, 37 years) and aged (61, 67, 69 years) human kidneys. GO enrichment map analysis of all proteins highlighted increased matrix and cell-matrix adhesion ontologies, and a reduction in mitochondrial components (**Figure 6A**). We found age associated increases in structural components collagen VI, fibulin-1, fibronectin and matrix regulators TIMP3 and ADAMTS5 (**Figure 6B**). Indeed several fibulin isoforms were increased in our mouse and human datasets and immunofluorescence confirmed increased fibulin-1 in the tubulointerstitium (**Figure 6C,D**). Furthermore, a number of age related changes were found in both glomerular and TI matrix including fibulin-1, TIMP3 and collagen VI (**Figure 7A,B**). There were also compartment distinct changes with reduced BM components observed in glomerular ageing but not seen in the aged TI matrix suggesting that tubular BMs are less exposed to damage during ageing. Relating these molecular changes to histology, we observed that ageing was only accompanied by a small increase in glomerulosclerosis and interstitial fibrosis and tubular

atrophy (IFTA) scores (**Figure 7C,D**), in keeping with our finding in the mouse disease models that altered matrix composition precedes overt or widespread structural changes.

A signature of altered kidney matrix in ageing and disease.

Across our ageing and disease datasets we observed consistent increases in collagen VI, nephronectin and fibrinogens and decreased BM components (**Figure 8A,B**). To investigate the relevance in human disease, we examined kidney biopsy sections from a young male patient with autosomal recessive Alport syndrome. Compared to control kidney sections, we observed increased levels of collagen VI and decreased levels of laminin-β2 in the glomerulus (**Figure 8C**). To determine whether this signature applied to a wider spectrum of human kidney disease, we searched for the signature proteins in published proteomic datasets. In a study of IgA nephropathy (11) we found consistency with increases in collagen VI and fibrinogen chains and in diabetic kidney disease (DKD) (12) there was increased collagen VI and nephronectin (**Figure 8D**). Data from a biopsy study of human focal segmental glomerulosclerosis (FSGS) identified increased interstitial collagen XV and Tgm2 (40). We also observed reduced BM components in IgA nephropathy and FSGS but not in DKD (**Figure 8D**), which may reflect the overall matrix expansion seen in DKD. To provide insight into the pathways associated with the matrix signature proteins, we created a 1-hop interaction network by connecting upregulated signature proteins with their nearest neighbours identified in protein interaction databases (**S.Figure 11**). This highlighted biological processes associated with matrix and adhesion but also with immune systems processes. We also compared the matrix signature proteins to RNA levels using the Nephroseq database and across a variety of phenotypes we observed similar increases in the signature transcripts (**Figure 8E, S.Table 3,4**). Finally we combined all primary, processed data from this study to allow direct evaluation (**S.Table 5**).

Discussion:

In this study we aimed to define altered matrix at the molecular level in kidney ageing and disease. We found: 1) ultrastructural change in matrix coupled with altered composition in models of glomerular disease, 2) similar patterns of altered glomerular matrix in human ageing with a reduction in BM proteins and an increase in interstitial matrix, 3) we defined the human tubulointerstitial matrix as a network of 141 components with a distinct pattern of altered matrix in ageing and 4) we observed a signature of altered matrix in kidney ageing and disease and provide evidence for shared pathobiology.

The processes that drive abnormal matrix in tissues remain unclear, although this understanding could lead to targeted therapies. In this study we describe altered matrix

structure with evolution over age and disease progression. The GBM of *Col4a3*$^{-/-}$ and *Col4a5*$^{-/-}$ mice at 6-8 weeks appeared normal, however proteomic analysis identified compositional change at this early stage. With age these disease models progressed with thickened GBM and the separation between control and disease matrix composition was more apparent. One aspect of the altered matrix was a reduction in BM components including collagen IV and laminins. In dynamic studies of endogenously tagged proteins in *C. elegans*, laminin and collagen IV orthologues have slower recovery after photobleaching compared to nidogens, agrin and perlecan (41). With this in mind, the reduction in BM components we observed could represent damage to these structures and an inability to replenish. We also observed increases in interstitial matrix with nephronectin and collagen VI, with integration of collagen VI into the GBM in *Col4a3*$^{-/-}$ mice. Genetic variants in *COL6A1/2/3* cause Bethlem and Ulrich myopathies (42) but no reported kidney phenotype. However, collagen VI degradation has been associated with chronic kidney disease (43) and its cleavage product endotrophin triggers fibrosis and metabolic dysfunction (44).

Glomerular capillaries are exposed to mechanical load during filtration. Loss of a key BM components may affect the mechanical properties of the GBM. Equally, loss of collagen VI has been shown to alter stiffness in the pericellular matrix of cartilage (45). Therefore collagen VI deposition in ageing and disease may occur to restore the mechanical properties of the GBM. Furthermore, collagen VI is a prominent downstream regulator of myofibroblast activity, with knockdown reducing fibrosis (46). Our data shows collagen VI increasing early where it may act to strengthen BM defects while paradoxically promoting fibrosis **(Figure 8E)**. However, the role of increased collagen VI requires further investigation as does the potential for targeted inhibition.

In parallel with altered matrix, we observed changes in cell adhesion components. The complex of proteins that assemble upon adhesion receptor and ligand engagement has been described for interactions with fibronectin (21) in addition to the BM ligands collagen IV and laminins (47). The consensus adhesome identified a series of four signalling hubs (38) and we found a global increase in components across all four signalling hubs. In addition, we found increases in receptors and their paired matrix ligand including integrin α1β1, integrin α2β1 with increased fibrillar collagens (I and III) and collagen VI and integrin α8β1 with nephronectin. Nephronectin is predominantly localized to the mesangium in the glomerulus and regulates mesangial cell adhesion (48), however increased GBM localization of nephronectin is reported in diabetic kidney disease (12). Our analysis of matrix receptors focussed on the integrin adhesion complexes as we did not detect discoid domain receptors (DDRs) or syndecans.

This could be due to low abundance or due to factors limiting their detection by mass spectrometry. Overall, the changes we observed in adhesion components could be explained by increased cell-matrix adhesion associated with podocyte effacement and increased interaction with the GBM.

To relate our findings in mice to human tissue, we investigated matrix isolated from young and older human kidneys. We also found a reduction in BM components and increased collagen VI and nephronectin in the aged glomerular matrix. Indeed, these components were also increased in proteomic studies of IgA nephropathy (11), DKD (12) and collagen VI was also upregulated in aged human dentin (49). A Nephroseq analysis provided further correlation between matrix signature proteins and transcriptional change in a variety of glomerular phenotypes. Kidney disease and ageing is associated with altered tubulointerstitial matrix and we therefore defined the human tubulointerstitial matrisome. We confirmed localization of 70% of these proteins in different kidney matrix compartments using the Human Protein Atlas and thereby demonstrate the value of proteomics for increasing the known composition of matrix compartments as an adjunct to immunolocalization. We further examined the change in tubulointerstitial matrix in ageing and defined a profile of altered matrix. Interestingly we did not observe the same reduction in stable BM components seen in the glomerular matrix and hypothesize this is due to differential mechanical load on glomerular and tubular BMs (50), although this could also depend on the pathological process and a reduction of BM components was recently descripted in a proteomic analysis of transplant kidney rejection (51).

In addition to resident kidney cells secreting abnormal matrix, transiting or infiltrating immune cells may also contribute. Macrophage to fibroblast crosstalk has been shown to direct new matrix synthesis and the direct contribution of macrophages to collagen scar formation in the heart is described in zebrafish (52). Starting with the matrix signature proteins we identified experimentally confirmed protein interactors and demonstrated 3 clusters of enriched biological processes. Unsurprisingly, these included cell matrix and cell adhesion, but also processes related to complement, TNF, NF_Kb and immune response to infection. These findings suggest that the signature of an altered matrix has greater interaction with immune system components than previously recognized.

In conclusion we describe a molecular basis for altered matrix in the kidney with common features across ageing and disease. Further investigations will focus on the cellular origins of the altered matrix and on the role of mechanical load on BM stability.

Author contribution statement: RL, MJR, JM, TVA, JN, DL, PP, MJH conceived and designed the studies, MJR, FL, QK, MKJ, PT, SF acquired the data, GR performed histological analysis on kidney sections. All the authors played an important role in interpreting the results, drafting and revising the manuscript. The authors have full access to the data in the study.

Acknowledgements: This work was supported by a Wellcome Trust Senior Fellowship award (202860/Z/16/Z) to R.L., a Kidney Research UK grant (RP52/2014) awarded to R.L and J.H.M to support a PDRA position for M.J.R and Cancer Research UK (C13329) and Wellcome Trust (092015) grants to M.J.H. D.A.L.'s laboratory is supported by the Medical Research Council (MR/P018629/1), Diabetes UK (13/0004763, 15/0005283, 17/0005733), Kidney Research UK (RP36/2015), and by the NIHR BRC at Great Ormond Street Hospital for Children NHS Foundation Trust and University College London. T.V.A's laboratory is supported by a Kidney Research UK (RP 19/2012), British Heart Foundation (PG/15/92/31813) and MRC (MR/R005567-1) grants. The authors also acknowledge core funding from the Wellcome Trust (203128/Z/16/Z) to the Wellcome Centre for Cell-Matrix Research at the University of Manchester. The mass spectrometer and microscopes used in this study were purchased with grants from the Biotechnology and Biological Sciences Research Council, the Wellcome Trust, and the University of Manchester Strategic Fund. MS was performed in the Biomolecular Analysis Core Facility, Faculty of Life Sciences, University of Manchester, and we thank David Knight and Stacey Warwood for advice and technical support and Julian Selley for bioinformatic support. The Bioimaging Facility microscopes used in this study were purchased with grants from BBSRC, Wellcome and the University of Manchester Strategic Fund. Special thanks goes to Peter March and Roger Meadows for their help with the microscopy. The authors thank the staff in the EM Core Facility in the Faculty of Biology, Medicine and Health for their assistance, and the Wellcome Trust for equipment grant support to the EM Core Facility.

Disclosure statement: RL is a consultant for Travere Therapeutics and receives studentship funding from GlaxoSmithKline. JN receives studentship funding from UCB and AstraZeneca. The other authors have nothing to declare.

Figure legends

Figure 1. Structural and compositional change in matrix. (a) Segmentation and modelling of serial block-face scanning electron microscopy data. Glomerular structure is visualized in Alport (*Col4a3*$^{-/-}$ and *Col4a5*$^{-/-}$) and *Col4a1*$^{+/SVC}$ mice. *Col4a1*$^{+/SVC}$ mice demonstrated splitting

of Bowman's capsule with enclosed nuclei. *Col4a3*$^{-/-}$ mice presented irregular GBM and progressive thickening of Bowman's capsule, whilst Bowman's capsule was conserved in the *Col4a5*$^{-/-}$ Alport mouse model. GBM (yellow), podocyte cell body with foot processes (light blue), Bowman's capsule basement membrane (green) were reconstructed. Dark blue lines highlight the thickness of the Bowman's capsule basement membrane. Nuclei of cells intercalate the basement membrane in *Col4a1*$^{+/SVC}$ are highlighted in pink. Note: The analysed *Col4a1*$^{+/SVC}$ received treatment with 4-Sodium phenyl butyric acid as described before which did not affect the kidney phenotype (38). (b) Quantification of GBM thickness; (c) podocyte foot process width (FPW); (d) Bowman's capsule basement membrane (BCBM) thickness. Young mice were aged 6-8 weeks (Y), adult mice were 16-18 weeks (A) and aged mice were 28 weeks old (A+). Box-and-whisker plots represent the median; box, interquartile range; whiskers, 10th to 90th percentile, n=1 biological sample per model. (e) Gene Ontology enrichment map analysis was performed on 719 proteins detected by mass spectrometry with altered abundance (>1.4 fold; p<0.1) in *Col4a1*$^{+/svc}$, *Col4a3*$^{-/-}$, *Col4a5*$^{-/-}$ mice at all analyzed ages compared with aged-matched control mice. Overrepresented biological process terms are presented as nodes, colour represents Bonferroni-corrected *p* value, the lower the *p* value the more intense the node colour. Edge weight represents overlap between the proteins in the connected nodes, n=5 biological samples per mouse model studied.

Figure 2. Evolution of altered matrix in ageing and disease. Mouse glomerular extracts were fractionated to cellular and matrix fractions. All fractions were analyzed by mass spectrometry, proteins were identified with Mascot and quantified using Progenesis. (a) Principal component analysis of all proteins detected was computed in Matlab. Components 1 and 2 are presented and the percentage variance explained by component 1 is indicated on the x-axis and by component 2 on the y-axis. Samples were fractionated and the matrix fraction was further analyzed. (b-e) Volcano plots of proteins detected in matrix fractions demonstrate differential expression shown as log2(fold change) compared to aged, matched control on the x-axis and -log10(p-value) on the y-axis. (b) *Col4a3*$^{-/-}$ 6-8 weeks (c) *Col4a3*$^{-/-}$ 16-18 weeks (d) *Col4a5*$^{-/-}$ 6-8 weeks (e) *Col4a5*$^{-/-}$ 16-18 weeks. (f) Detected matrix proteins at the 6-8 weeks were clustered in MeV using Euclidean distance complete linkage. The clustered dendrogram is presented as a heatmap with orange representing increased abundance in Col4a mutant relative to control.

Figure 3: Altered matrix localization in Alport syndrome. Immunofluorescence demonstrated reduced BM proteins and increased interstitial matrix proteins in Alport mouse glomeruli. (a) Kidney sections of 8 week old *Col4a5*$^{-/-}$ and wildtype mice were immunolabeled

for collagen 1, collagen VI, laminin-β2, Tinag and nidogen. Scale bar is 20 μm. (b) Quantification of (a). Mean fluorescence intensity was normalized to background and measured using ImageJ software. Images were acquired from n= 4 mice per genotype and between 10-15 glomeruli were analyzed per mouse, pooled data are shown. (c) Stochastic optical reconstruction microscopy was performed for integrin-β1 (green) and collagen VI (purple) on *Col4a3*$^{+/-}$ and *Col4a3*$^{-/-}$ mouse sections. Region of interest (ROI) highlights collagen VI localization to the GBM in *Col4a3*$^{-/-}$ glomeruli. Scale bar represents 2 micrometres.

Figure 4: Altered cell-matrix adhesion components. Unsupervised hierarchical clustered heatmap displaying the fold enrichment of adhesion proteins detected in 6-8 week *Col4a1*$^{+/svc}$, *Col4a3*$^{-/-}$, *Col4a5*$^{-/-}$ mass spectrometry datasets compared to their respective control, orange (+ is increased abundance in disease relative to control) blue (- represents decreased abundance in disease relative to control). Adhesion proteins are displayed along the four different signalling axes to the actin cytoskeleton as described previously (38).

Figure 5: Distinct matrix composition in human glomerular ageing. Glomeruli were isolated from young (15, 29, 37 years) and aged (61, 67, 69 years) human kidneys, subjected to matrix fractionation and analyzed by mass spectrometry. (a) Principal component analysis of matrisome proteins was carried out in Matlab, components 1 and 2 are presented and the percentage variance explained by each component is indicated on the relevant axis. (b) Volcano plots of proteins detected in matrix fractions demonstrate differential protein abundance shown as log2(fold change) glomerular aged over glomerular young on the x-axis and -log10(p-value) on the y-axis. (c) Unsupervised hierarchical clustered heatmap displaying extracellular matrix proteins detected in young and aged glomerular datasets. Data was standardised by row z-score and grouped in MeV using Pearson correlation complete linkage clustering. Inset line graph shows increased type VI collagen protein abundance with age. (d) Mass spectrometry data from matrix enriched protein fractions were filtered for known matrisome proteins. These proteins were mapped onto a merged human, mouse and rat interactome. Protein-protein interaction network of altered human glomerular matrisome proteins. Nodes represent proteins and edges represent reported protein-protein interactions. Colour represents fold enrichment to datasets, with increased abundance in aged human glomerular samples illustrated in red and increased abundance in young human glomerular samples illustrated in blue. Proteins are grouped by function.

Figure 6: Molecular characterization of tubulointerstitial change in ageing. Tubulointerstitial matrix was isolated from *young* (15, 29, 37 years) and *aged* (61, 67, 69 years)

human kidney samples. (a) Volcano plots of proteins detected in extracellular matrix fractions demonstrate differential protein abundance shown as log2(fold change) tubulointerstitial aged over tubulointerstitial young on the x-axis and -log10(p-value) on the y-axis. (b) Unsupervised hierarchical clustered heatmap displaying extracellular matrix proteins detected in young and aged glomerular datasets. Data was standardised by row z-score and grouped in MeV using Pearson correlation complete linkage clustering. Inset line graph shows increased collagen VI protein abundance with age. (c) Mass spectrometry data from matrix enriched protein fractions were filtered for known matrisome proteins. These proteins were mapped onto a merged human, mouse and rat interactome. Protein-protein interaction network of altered human tubulointerstitial matrisome proteins. Nodes represent proteins and edges represent reported protein-protein interactions. Colour represents fold enrichment to datasets, with increased abundance in aged human tubulointerstitial samples illustrated in red and increased abundance in young human tubulointerstitial samples illustrated in blue. Proteins are grouped functionally. (d) Sections of normal human kidneys were stained with an antibody to fibulin-1 (red) and nuclei were stained with Hoechst 33342 (blue). Representative images are shown. Magnification: left panel x40, right panel x20. (e) The fluorescent signal in 20 fields/kidney was quantified using ImageJ. ***: P value < 0.0005. ****: P value < 0.0001.

Figure 7: Comparison of the glomerular and tubulointerstitial matrix in ageing. (a) Unsupervised hierarchical clustered heatmap displaying extracellular matrix proteins detected in human glomerular and tubulointerstitial samples analysed by mass spectrometry. Data were standardized by row z-score, clustered using Pearson uncentered distance matrix and visualized in MeV. Comparison of human glomerular and human tubulointerstitial matrix proteins with age. Line graphs show laminin proteins with increased abundance in the human glomerular matrix relative to human tubulointerstitial samples. (b) Volcano plots of proteins detected in extracellular matrix fractions demonstrate differential protein abundance shown as log2(fold change) glomerular over tubulointerstitium on the x-axis and -log10(p-value) on the y-axis. (c) TriPAS staining of young and older kidney sections highlighting increased matrix in the older kidney section. Scale bar represents 100μm. (d) Glomerulosclerosis and interstitial fibrosis and tubular atrophy (IFTA) scoring in n=3 young and n=3 aged kidneys.

Figure 8: A signature of altered kidney matrix in ageing and disease. (a,b) Bar graph displaying protein fold change of consistently altered matrix signature proteins relative to their respective controls. Error bars represent standard deviation. #p<0.1, *p<0.05, **p<0.01, ***p<0.001. (a) upregulated signature proteins. (b) downregulated signature proteins. (c) Biopsy sections from a patient with autosomal recessive Alport syndrome case and Ctrl kidney

tissue (non-affected tissue of a tumor nephrectomy sample) were stained for type VI collagen, laminin beta 2 and nephrin. Scale bar is 50 μm (d) Dot plot comparison of signature matrix proteins to their protein levels in microdissected human IgA nephropathy samples (IgAN total and progressive IgAN) (11), human diabetic samples (12) and human FSGS samples (collapsing FSGS and FSGS not otherwise specified) (40) Significance ($p<0.05$) is indicated by an asterisk proximal to the datapoint. Fold change is presented on the y axis and dataset is highlighted by colour. (e) Analysis of signature protein transcript levels in different disease datasets using Nephroseq v5 database. Glomerular datasets were extracted and altered transcript levels with fold change +/- 1.5 and $p<0.05$ are shown. The % detection of searched gene transcript is shown (number of datasets = 21). Full details for Nephroseq datasets and transcript fold changes used for each signature gene can be found in **S.Table 4**. (f) Schematic of hypothesized basement membrane injury process.

Supplemental material Table of Contents

Supplemental Videos

Supplemental Tables

Table S4: Nephroseq v5 analysis.

Table S5: Normalized abundance for all primary datasets.

References

1. Yurchenco PD: Basement membranes: cell scaffoldings and signaling platforms. *Cold Spring Harbor perspectives in biology,* 3, 2011 10.1101/cshperspect.a004911
2. Li X, Chen Y, Schéele S, Arman E, Haffner-Krausz R, Ekblom P, et al.: Fibroblast growth factor signaling and basement membrane assembly are connected during epithelial morphogenesis of the embryoid body. *J Cell Biol,* 153**:** 811-822, 2001 10.1083/jcb.153.4.811
3. Naba A, Clauser KR, Hoersch S, Liu H, Carr SA, Hynes RO: The matrisome: in silico definition and in vivo characterization by proteomics of normal and tumor extracellular matrices. *Molecular & cellular proteomics : MCP,* 11**:** M111 014647, 2012 10.1074/mcp.M111.014647
4. Wynn TA: Cellular and molecular mechanisms of fibrosis. *J Pathol,* 214**:** 199-210, 2008 10.1002/path.2277
5. Haas M, Rastaldi MP, Fervenza FC: Histologic classification of glomerular diseases: clinicopathologic correlations, limitations exposed by validation studies, and suggestions for modification. *Kidney Int,* 86**:** 648, 2014 10.1038/ki.2014.230
6. Remuzzi G, Bertani T: Is glomerulosclerosis a consequence of altered glomerular permeability to macromolecules? *Kidney Int,* 38**:** 384-394, 1990 10.1038/ki.1990.217
7. Zeisberg M, Neilson EG: Mechanisms of tubulointerstitial fibrosis. *J Am Soc Nephrol,* 21**:** 1819-1834, 2010 10.1681/ASN.2010080793
8. O'Sullivan ED, Hughes J, Ferenbach DA: Renal Aging: Causes and Consequences. *J Am Soc Nephrol,* 28**:** 407-420, 2017 10.1681/ASN.2015121308
9. Lennon R, Byron A, Humphries JD, Randles MJ, Carisey A, Murphy S, et al.: Global analysis reveals the complexity of the human glomerular extracellular matrix. *J Am Soc Nephrol,* 25**:** 939-951, 2014 10.1681/ASN.2013030233
10. Hobeika L, Barati MT, Caster DJ, McLeish KR, Merchant ML: Characterization of glomerular extracellular matrix by proteomic analysis of laser-captured microdissected glomeruli. *Kidney Int,* 91**:** 501-511, 2017 10.1016/j.kint.2016.09.044
11. Paunas FTI, Finne K, Leh S, Osman TA, Marti HP, Berven F, et al.: Characterization of glomerular extracellular matrix in IgA nephropathy by proteomic analysis of laser-captured microdissected glomeruli. *BMC Nephrol,* 20**:** 410, 2019 10.1186/s12882-019-1598-1

12. Nakatani S, Wei M, Ishimura E, Kakehashi A, Mori K, Nishizawa Y, et al.: Proteome analysis of laser microdissected glomeruli from formalin-fixed paraffin-embedded kidneys of autopsies of diabetic patients: nephronectin is associated with the development of diabetic glomerulosclerosis. *Nephrol Dial Transplant,* 27**:** 1889-1897, 2012 10.1093/ndt/gfr682
13. Randles MJ, Humphries MJ, Lennon R: Proteomic definitions of basement membrane composition in health and disease. *Matrix Biol,* 57-58**:** 12-28, 2017 10.1016/j.matbio.2016.08.006
14. Miner JH: Renal basement membrane components. *Kidney international,* 56**:** 2016-2024, 1999 10.1046/j.1523-1755.1999.00785.x
15. Khoshnoodi J, Pedchenko V, Hudson BG: Mammalian collagen IV. *Microsc Res Tech,* 71**:** 357-370, 2008 10.1002/jemt.20564
16. Van Agtmael T, Schlötzer-Schrehardt U, McKie L, Brownstein DG, Lee AW, Cross SH, et al.: Dominant mutations of Col4a1 result in basement membrane defects which lead to anterior segment dysgenesis and glomerulopathy. *Hum Mol Genet,* 14**:** 3161-3168, 2005 10.1093/hmg/ddi348
17. Miner JH, Sanes JR: Molecular and functional defects in kidneys of mice lacking collagen alpha 3(IV): implications for Alport syndrome. *J Cell Biol,* 135**:** 1403-1413, 1996
18. Dickinson ME, Flenniken AM, Ji X, Teboul L, Wong MD, White JK, et al.: High-throughput discovery of novel developmental phenotypes. *Nature,* 537**:** 508-514, 2016 10.1038/nature19356
19. IMP C: Allele Col4a5 tm1a(EUCOMM)Wtsi, Available at:.
20. Shevchenko A, Wilm M, Vorm O, Mann M: Mass spectrometric sequencing of proteins silver-stained polyacrylamide gels. *Anal Chem,* 68**:** 850-858, 1996
21. Humphries JD, Byron A, Bass MD, Craig SE, Pinney JW, Knight D, et al.: Proteomic analysis of integrin-associated complexes identifies RCC2 as a dual regulator of Rac1 and Arf6. *Science signaling,* 2**:** ra51, 2009 10.1126/scisignal.2000396
22. Nesvizhskii AI, Keller A, Kolker E, Aebersold R: A statistical model for identifying proteins by tandem mass spectrometry. *Analytical chemistry,* 75**:** 4646-4658, 2003
23. Zaidel-Bar R, Geiger B: The switchable integrin adhesome. *Journal of cell science,* 123**:** 1385-1388, 2010 10.1242/jcs.066183
24. Berthier CC, Bethunaickan R, Gonzalez-Rivera T, Nair V, Ramanujam M, Zhang W, et al.: Cross-species transcriptional network analysis defines shared inflammatory responses in murine and human lupus nephritis. *J Immunol,* 189**:** 988-1001, 2012 10.4049/jimmunol.1103031

25. Hodgin JB, Nair V, Zhang H, Randolph A, Harris RC, Nelson RG, et al.: Identification of cross-species shared transcriptional networks of diabetic nephropathy in human and mouse glomeruli. *Diabetes,* 62**:** 299-308, 2013 10.2337/db11-1667

26. Hodgin JB, Borczuk AC, Nasr SH, Markowitz GS, Nair V, Martini S, et al.: A molecular profile of focal segmental glomerulosclerosis from formalin-fixed, paraffin-embedded tissue. *Am J Pathol,* 177**:** 1674-1686, 2010 10.2353/ajpath.2010.090746

27. Neusser MA, Lindenmeyer MT, Moll AG, Segerer S, Edenhofer I, Sen K, et al.: Human nephrosclerosis triggers a hypoxia-related glomerulopathy. *Am J Pathol,* 176**:** 594-607, 2010 10.2353/ajpath.2010.090268

28. Peterson KS, Huang JF, Zhu J, D'Agati V, Liu X, Miller N, et al.: Characterization of heterogeneity in the molecular pathogenesis of lupus nephritis from transcriptional profiles of laser-captured glomeruli. *J Clin Invest,* 113**:** 1722-1733, 2004 10.1172/JCI19139

29. Reich HN, Tritchler D, Cattran DC, Herzenberg AM, Eichinger F, Boucherot A, et al.: A molecular signature of proteinuria in glomerulonephritis. *PLoS One,* 5**:** e13451, 2010 10.1371/journal.pone.0013451

30. Woroniecka KI, Park AS, Mohtat D, Thomas DB, Pullman JM, Susztak K: Transcriptome analysis of human diabetic kidney disease. *Diabetes,* 60**:** 2354-2369, 2011 10.2337/db10-1181

31. Starborg T, Kalson NS, Lu Y, Mironov A, Cootes TF, Holmes DF, et al.: Using transmission electron microscopy and 3View to determine collagen fibril size and three-dimensional organization. *Nat Protoc,* 8**:** 1433-1448, 2013 10.1038/nprot.2013.086

32. Jones FE, Murray LS, McNeilly S, Dean A, Aman A, Lu Y, et al.: 4-Sodium phenyl butyric acid has both efficacy and counter-indicative effects in the treatment of Col4a1 disease. *Hum Mol Genet,* 28**:** 628-638, 2019 10.1093/hmg/ddy369

33. Suleiman H, Zhang L, Roth R, Heuser JE, Miner JH, Shaw AS, et al.: Nanoscale protein architecture of the kidney glomerular basement membrane. *Elife,* 2**:** e01149, 2013 10.7554/eLife.01149

34. Suleiman HY, Roth R, Jain S, Heuser JE, Shaw AS, Miner JH: Injury-induced actin cytoskeleton reorganization in podocytes revealed by super-resolution microscopy. *JCI Insight,* 2, 2017 10.1172/jci.insight.94137

35. Vizcaino JA, Csordas A, Del-Toro N, Dianes JA, Griss J, Lavidas I, et al.: 2016 update of the PRIDE database and its related tools. *Nucleic Acids Res,* 44**:** 11033, 2016 10.1093/nar/gkw880

36. Jones FE, Bailey MA, Murray LS, Lu Y, McNeilly S, Schlötzer-Schrehardt U, et al.: ER stress and basement membrane defects combine to cause glomerular and tubular

renal disease resulting from Col4a1 mutations in mice. *Dis Model Mech,* 9**:** 165-176, 2016 10.1242/dmm.021741

37. Tsuji K, Suleiman H, Miner JH, Daley JM, Capen DE, Păunescu TG, et al.: Ultrastructural Characterization of the Glomerulopathy in Alport Mice by Helium Ion Scanning Microscopy (HIM). *Sci Rep,* 7**:** 11696, 2017 10.1038/s41598-017-12064-5
38. Horton ER, Byron A, Askari JA, Ng DHJ, Millon-Frémillon A, Robertson J, et al.: Definition of a consensus integrin adhesome and its dynamics during adhesion complex assembly and disassembly. *Nat Cell Biol,* 17**:** 1577-1587, 2015 10.1038/ncb3257
39. Uhlen M, Oksvold P, Fagerberg L, Lundberg E, Jonasson K, Forsberg M, et al.: Towards a knowledge-based Human Protein Atlas. *Nature biotechnology,* 28**:** 1248-1250, 2010 10.1038/nbt1210-1248
40. Merchant ML, Barati MT, Caster DJ, Hata JL, Hobeika L, Coventry S, et al.: Proteomic Analysis Identifies Distinct Glomerular Extracellular Matrix in Collapsing Focal Segmental Glomerulosclerosis. *J Am Soc Nephrol*, 2020 10.1681/ASN.2019070696
41. Keeley DP, Hastie E, Jayadev R, Kelley LC, Chi Q, Payne SG, et al.: Comprehensive Endogenous Tagging of Basement Membrane Components Reveals Dynamic Movement within the Matrix Scaffolding. *Dev Cell*, 2020 10.1016/j.devcel.2020.05.022
42. Bonnemann CG: The collagen VI-related myopathies Ullrich congenital muscular dystrophy and Bethlem myopathy. *Handbook of clinical neurology / edited by PJ Vinken and GW Bruyn,* 101**:** 81-96, 2011 10.1016/B978-0-08-045031-5.00005-0
43. Rasmussen DGK, Boesby L, Nielsen SH, Tepel M, Birot S, Karsdal MA, et al.: Collagen turnover profiles in chronic kidney disease. *Sci Rep,* 9**:** 16062, 2019 10.1038/s41598-019-51905-3
44. Sun K, Park J, Gupta OT, Holland WL, Auerbach P, Zhang N, et al.: Endotrophin triggers adipose tissue fibrosis and metabolic dysfunction. *Nat Commun,* 5**:** 3485, 2014 10.1038/ncomms4485
45. Alexopoulos LG, Youn I, Bonaldo P, Guilak F: Developmental and osteoarthritic changes in Col6a1-knockout mice: biomechanics of type VI collagen in the cartilage pericellular matrix. *Arthritis Rheum,* 60**:** 771-779, 2009 10.1002/art.24293
46. Williams LM, McCann FE, Cabrita MA, Layton T, Cribbs A, Knezevic B, et al.: Identifying collagen VI as a target of fibrotic diseases regulated by CREBBP/EP300. *Proc Natl Acad Sci U S A,* 117**:** 20753-20763, 2020 10.1073/pnas.2004281117
47. Randles MJ, Lausecker F, Humphries JD, Byron A, Clark SJ, Miner JH, et al.: Basement membrane ligands initiate distinct signalling networks to direct cell shape. *Matrix Biol*, 2020 10.1016/j.matbio.2020.02.005

48. Zimmerman SE, Hiremath C, Tsunezumi J, Yang Z, Finney B, Marciano DK: Nephronectin Regulates Mesangial Cell Adhesion and Behavior in Glomeruli. *J Am Soc Nephrol,* 29**:** 1128-1140, 2018 10.1681/ASN.2017070752

49. Reis M, Lee F, Bedran-Russo AK, Naba A: Proteomic Profiling of the Human Dentin Identifies Age-Related Differences in the Composition and Solubility of the Matrisome. *BioRxiv*, 2020 https://doi.org/10.1101/2020.05.27.116624

50. Kriz W, Lemley KV: A potential role for mechanical forces in the detachment of podocytes and the progression of CKD. *J Am Soc Nephrol,* 26**:** 258-269, 2015 10.1681/ASN.2014030278

51. Clotet-Freixas S, McEvoy CM, Batruch I, Pastrello C, Kotlyar M, Van JAD, et al.: Extracellular Matrix Injury of Kidney Allografts in Antibody-Mediated Rejection: A Proteomics Study. *J Am Soc Nephrol,* 31**:** 2705-2724, 2020 10.1681/ASN.2020030286

52. Simões FC, Cahill TJ, Kenyon A, Gavriouchkina D, Vieira JM, Sun X, et al.: Macrophages directly contribute collagen to scar formation during zebrafish heart regeneration and mouse heart repair. *Nat Commun,* 11**:** 600, 2020 10.1038/s41467-019-14263-2

Significance statement

Abnormal extracellular matrix is a histological feature of kidney ageing and disease, however a comprehensive molecular basis for altered matrix is lacking. Combining ultrastructural and proteomic studies in mouse models of genetic kidney disease and human tissue, this study defines a molecular basis for altered matrix, which has common features across ageing and disease progression. Broadly there is a reduction of basement membrane components and an increase in interstitial matrix proteins coupled with altered cell adhesion and metabolic processes. Furthermore, a signature of altered matrix proteins appears prior to ultrastructural defects and could have utility as biomarkers of kidney health. Mechanistically, this altered kidney matrix may initiate abnormal kidney cell-matrix and immune cell-matrix interactions, which could be targeted by therapy.

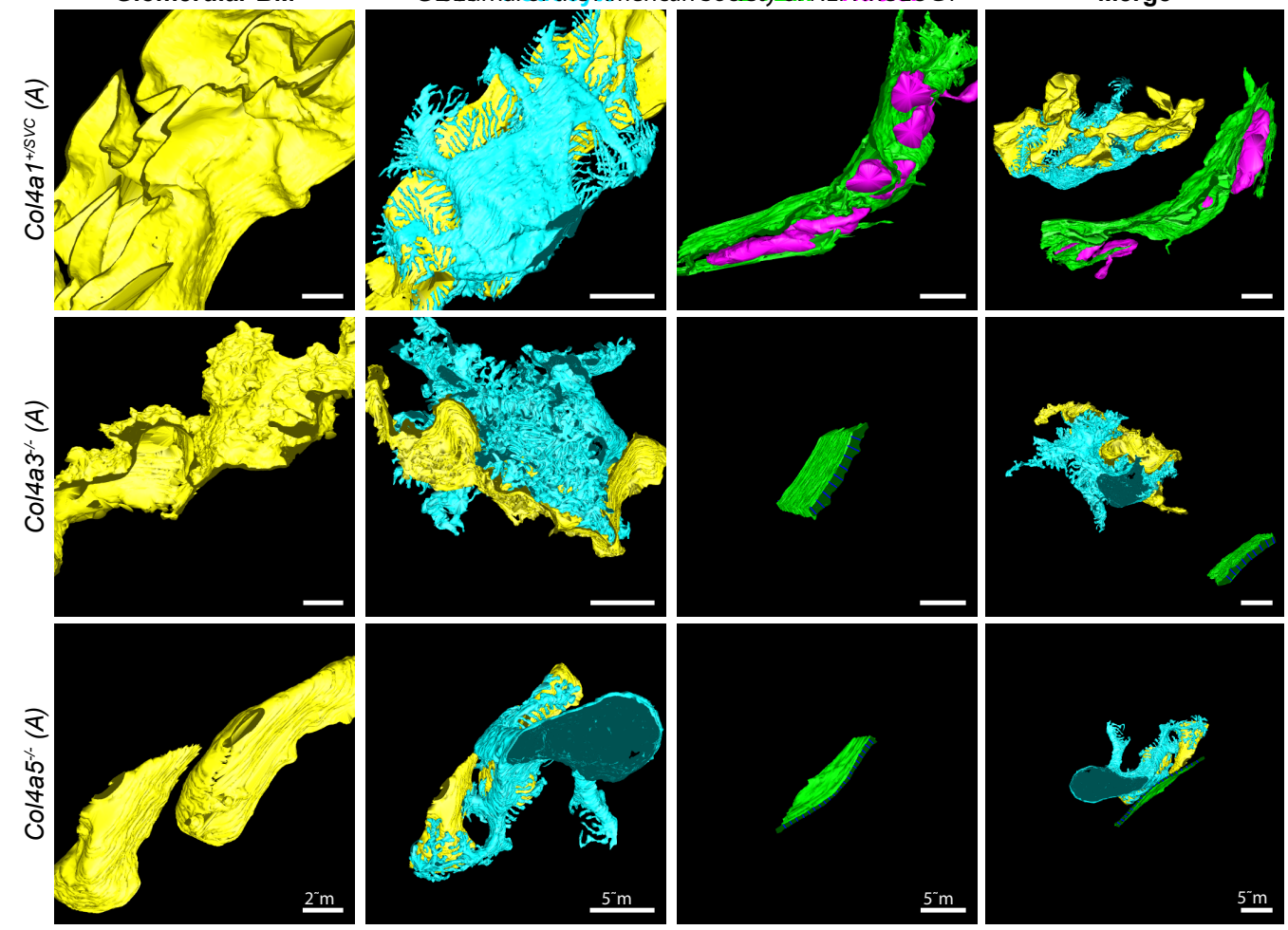

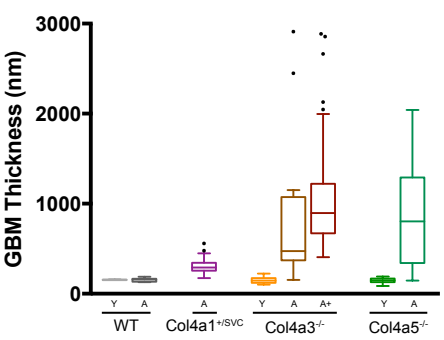

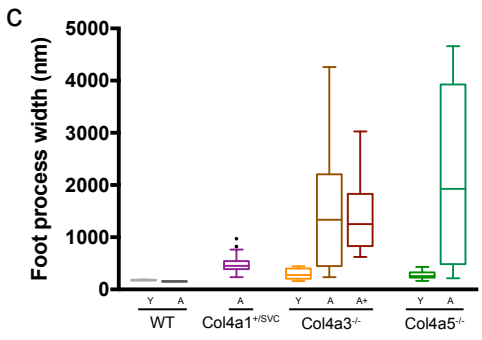

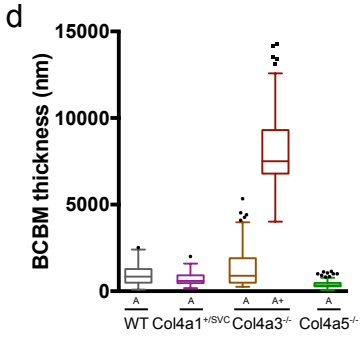

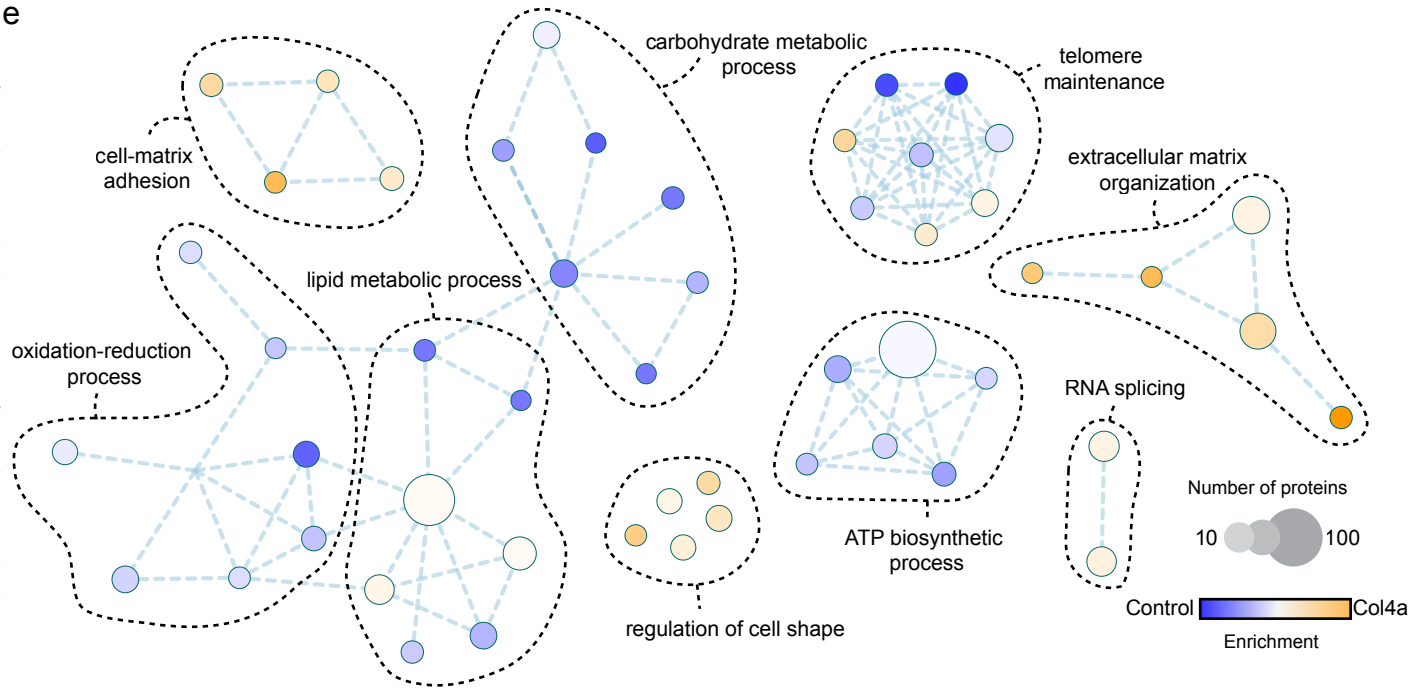

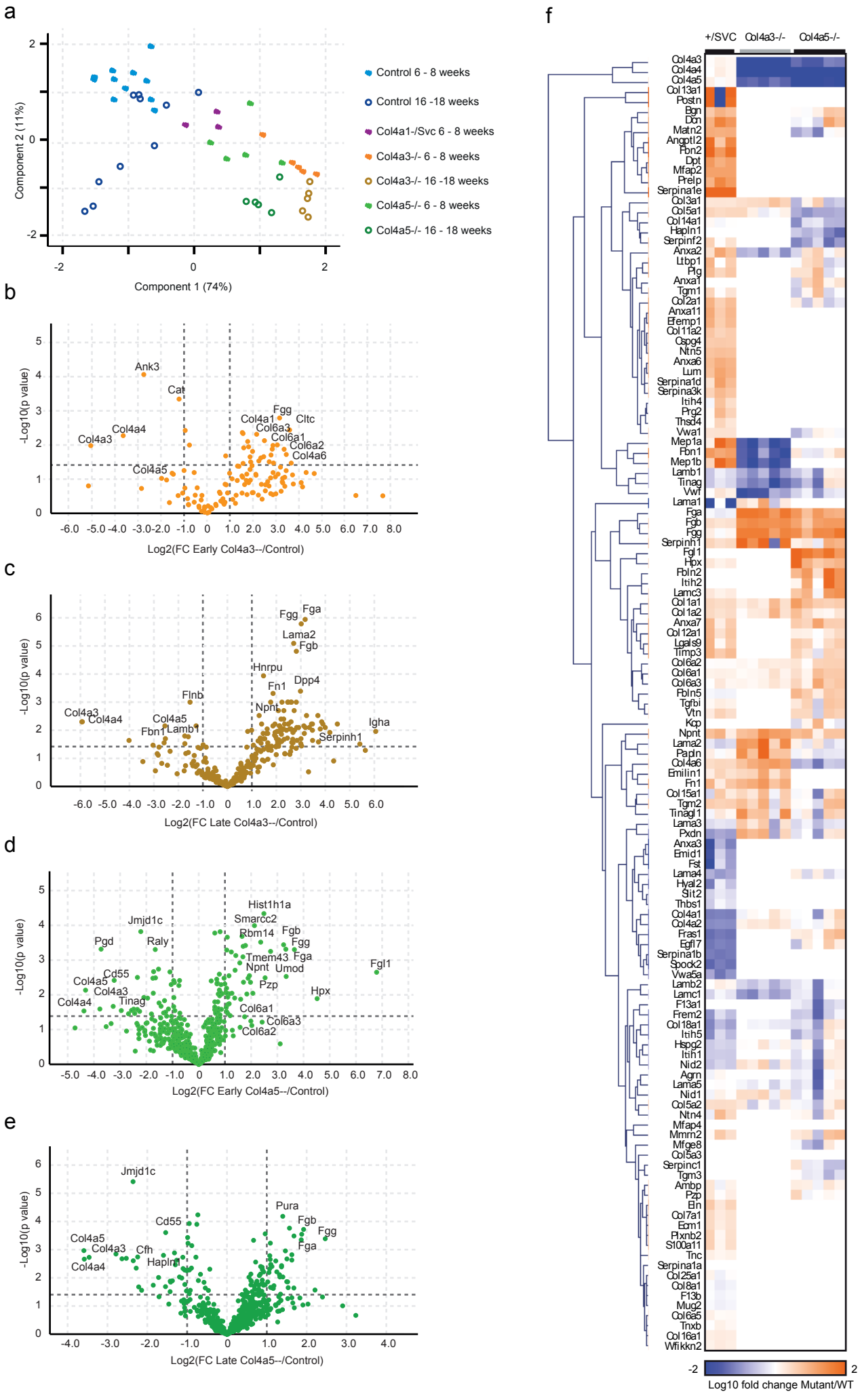
a
Component 2 (11%)
Component 1 (74%)
Control 6 - 8 weeks
Control 16 -18 weeks
Col4a1-/Svc 6 - 8 weeks
Col4a3-/- 6 - 8 weeks
Col4a3-/- 16 -18 weeks
Col4a5-/- 6 - 8 weeks
Col4a5-/- 16 - 18 weeks
b
-Log10(p value)
Log2(FC Early Col4a3--/Control)
Ank3
Cat
Fgg
Col4a1
Cltc
Col6a3
Col4a4
Col4a3
Col6a1
Col6a2
Col4a6
Col4a5
c
-Log10(p value)
Log2(FC Late Col4a3--/Control)
Fgg
Fga
Lama2
Fgb
Hnrpu
Dpp4
Fn1
Flnb
Npnt
Col4a3
Col4a4
Col4a5
Fbn1
Lamb1
Igha
Serpinh1
d
-Log10(p value)
Log2(FC Early Col4a5--/Control)
Hist1h1a
Jmjd1c
Smarcc2
Rbm14
Fgb
Pgd
Raly
Fgg
Tmem43
Fga
Fgl1
Npnt
Umod
Cd55
Col4a5
Pzp
Col4a3
Hpx
Col4a4
Tinag
Col6a1
Col6a3
Col6a2
e
-Log10(p value)
Log2(FC Late Col4a5--/Control)
Jmjd1c
Pura
Cd55
Fgb
Fgg
Col4a5
Col4a3
Cfh
Fga
Col4a4
Hapln1
f
+/SVC
Col4a3-/-
Col4a5-/-
Col4a3
Col4a4
Col4a5
Col13a1
Postn
Bgn
Dcn
Matn2
Angptl2
Fbn2
Dpt
Mfap2
Prelp
Serpina1e
Col3a1
Col5a1
Col14a1
Hapln1
Serpinf2
Anxa2
Ltbp1
Ptg
Anxa1
Tgm1
Col2a1
Anxa11
Efemp1
Col11a2
Cspg4
Ntn5
Anxa6
Lum
Serpina1d
Serpina3k
Itih4
Prg2
Thsd4
Vwa1
Mep1a
Fbn1
Mep1b
Lamb1
Tinag
Vwf
Lama1
Fga
Fgb
Fgg
Serpinh1
Fgl1
Hpx
Fbln2
Itih2
Lamc3
Col1a1
Col1a2
Anxa7
Col12a1
Lgals9
Timp3
Col6a2
Col6a1
Col6a3
Fbln5
Tgfbi
Vtn
Kcp
Npnt
Lama2
Papln
Col4a6
Emilin1
Fn1
Col15a1
Tgm2
Tinagl1
Lama3
Pxdn
Anxa3
Emid1
Fst
Lama4
Hyal2
Slit2
Thbs1
Col4a1
Col4a2
Fras1
Egfl7
Serpina1b
Spock2
Vwa5a
Lamb2
Lamc1
F13a1
Frem2
Col18a1
Itih5
Hspg2
Itih1
Nid2
Agrn
Lama5
Nid1
Col5a2
Ntn4
Mfap4
Mmrn2
Mfge8
Col5a3
Serpinc1
Tgm3
Ambp
Pzp
Eln
Col7a1
Ecm1
Plxnb2
S100a11
Tnc
Serpina1a
Col25a1
Col8a1
F13b
Mug2
Col6a5
Tnxb
Col16a1
Wfikkn2
-2
2
Log10 fold change Mutant/WT

Figure 3

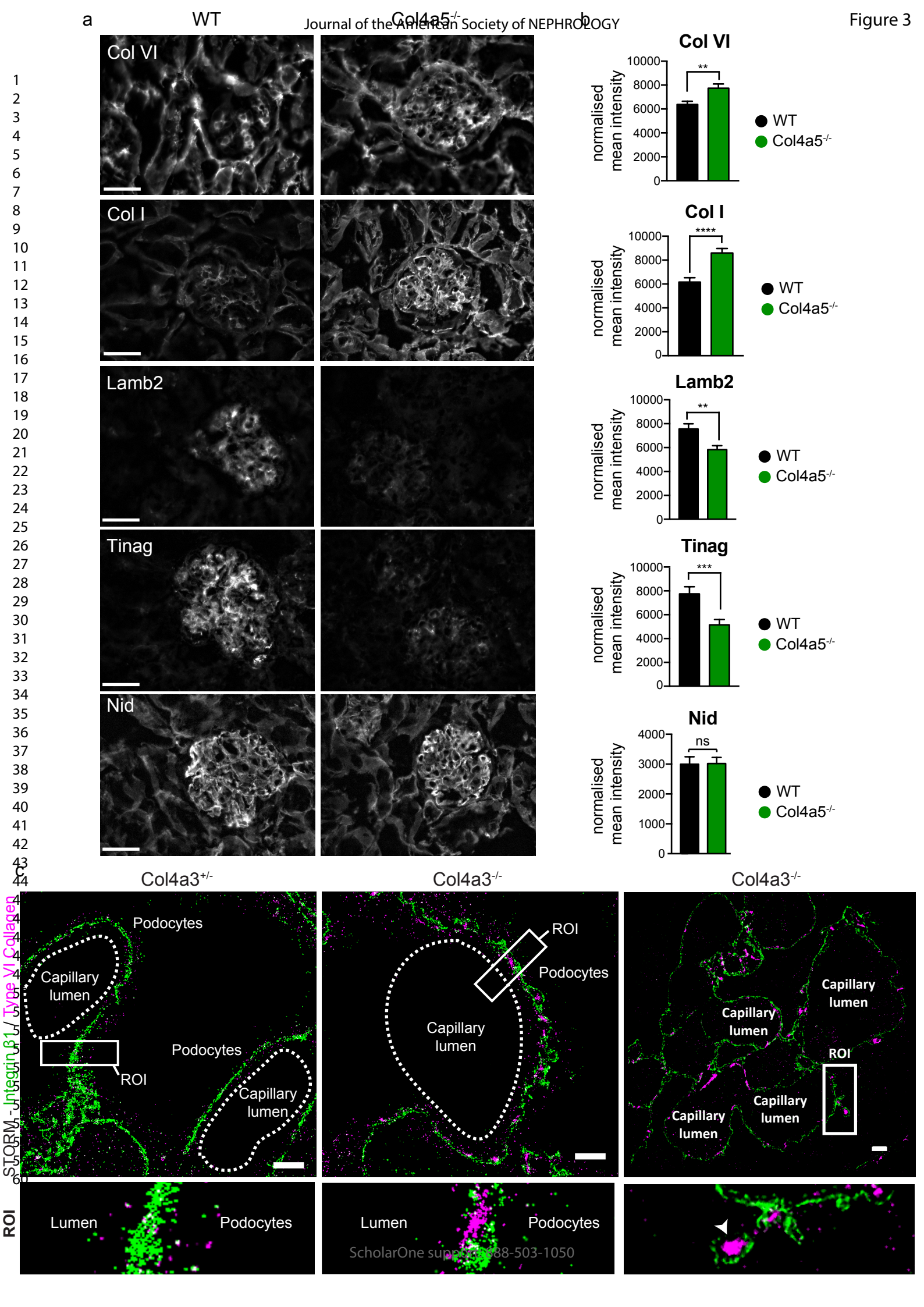

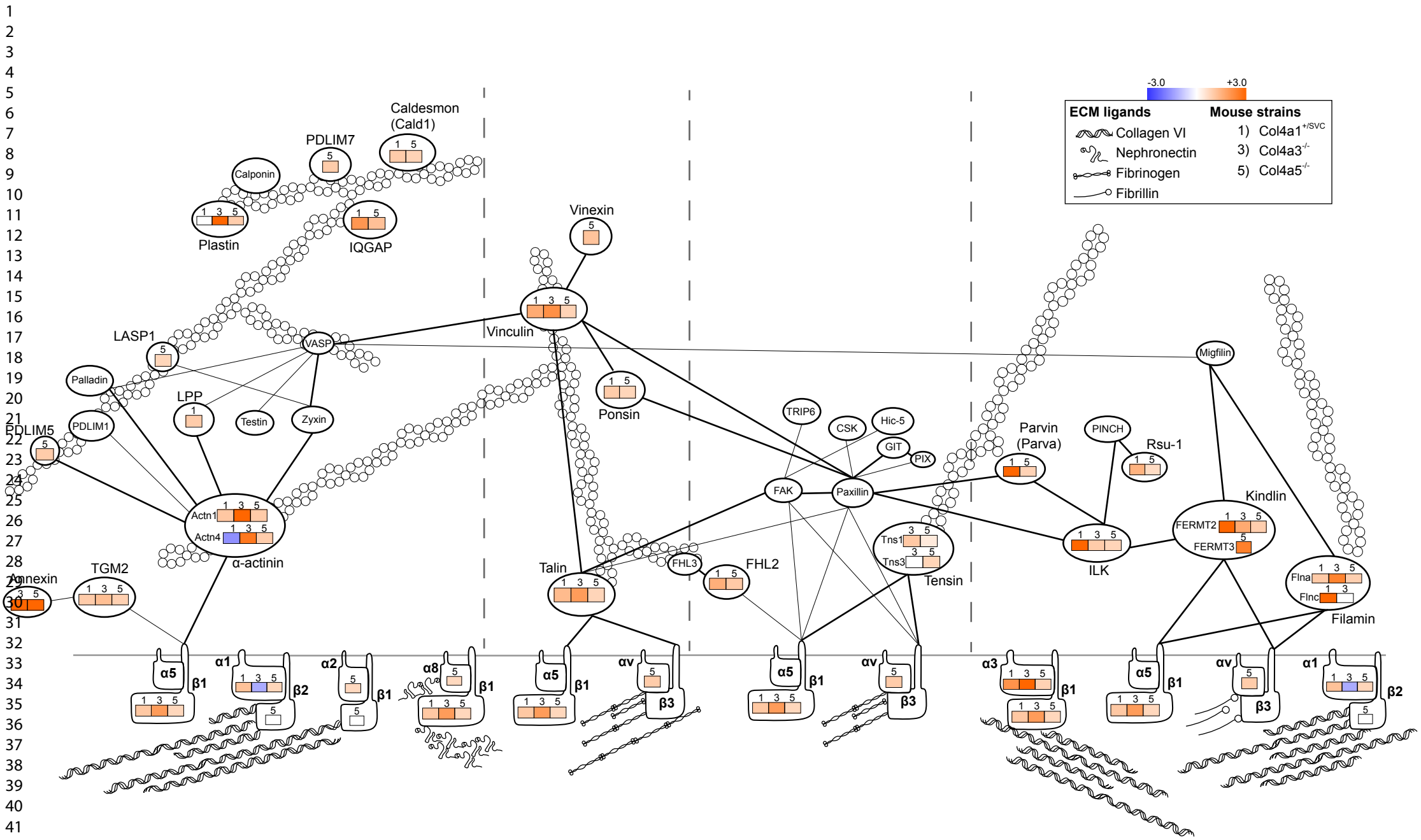
-3.0
+3.0
ECM ligands
Collagen VI
Nephronectin
Fibrinogen
Fibrillin
Mouse strains
1) Col4a1+/SVC
3) Col4a3-/-
5) Col4a5-/-
Caldesmon (Cald1)
PDLIM7
Calponin
Plastin
IQGAP
Vinexin
Vinculin
LASP1
VASP
Palladin
LPP
Testin
Zyxin
PDLIM1
PDLIM5
Ponsin
TRIP6
CSK
Hic-5
GIT
PIX
FAK
Paxillin
Parvin (Parva)
PINCH
Rsu-1
Migfilin
Kindlin
FERMT2
FERMT3
ILK
Tns1
Tns3
Tensin
Actn1
Actn4
α-actinin
Talin
FHL3
FHL2
Annexin
TGM2
Flna
Flnc
Filamin
α1
α2
α3
α5
α8
αv
β1
β2
β3

Figure 5

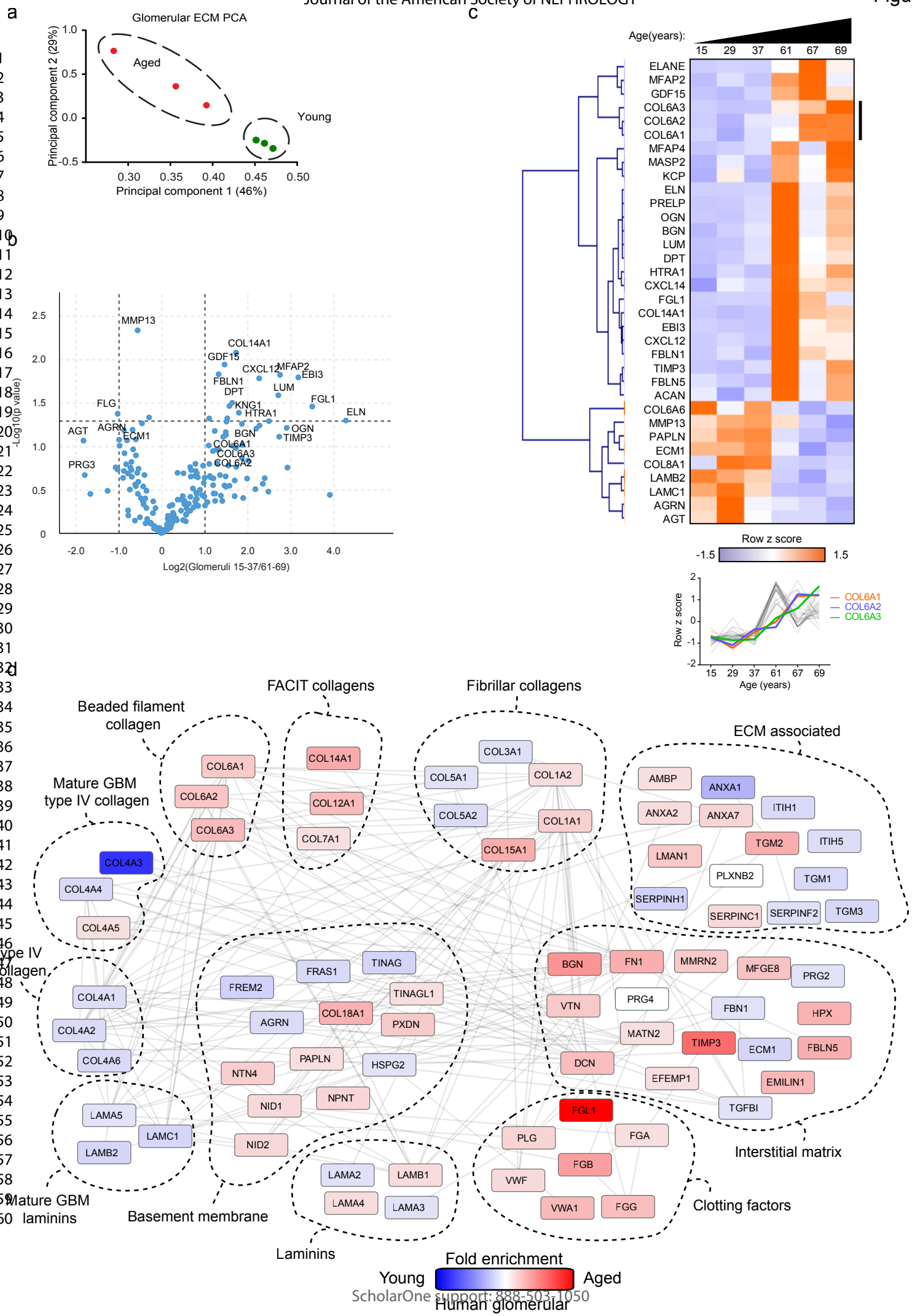

Human glomerular matrix over age

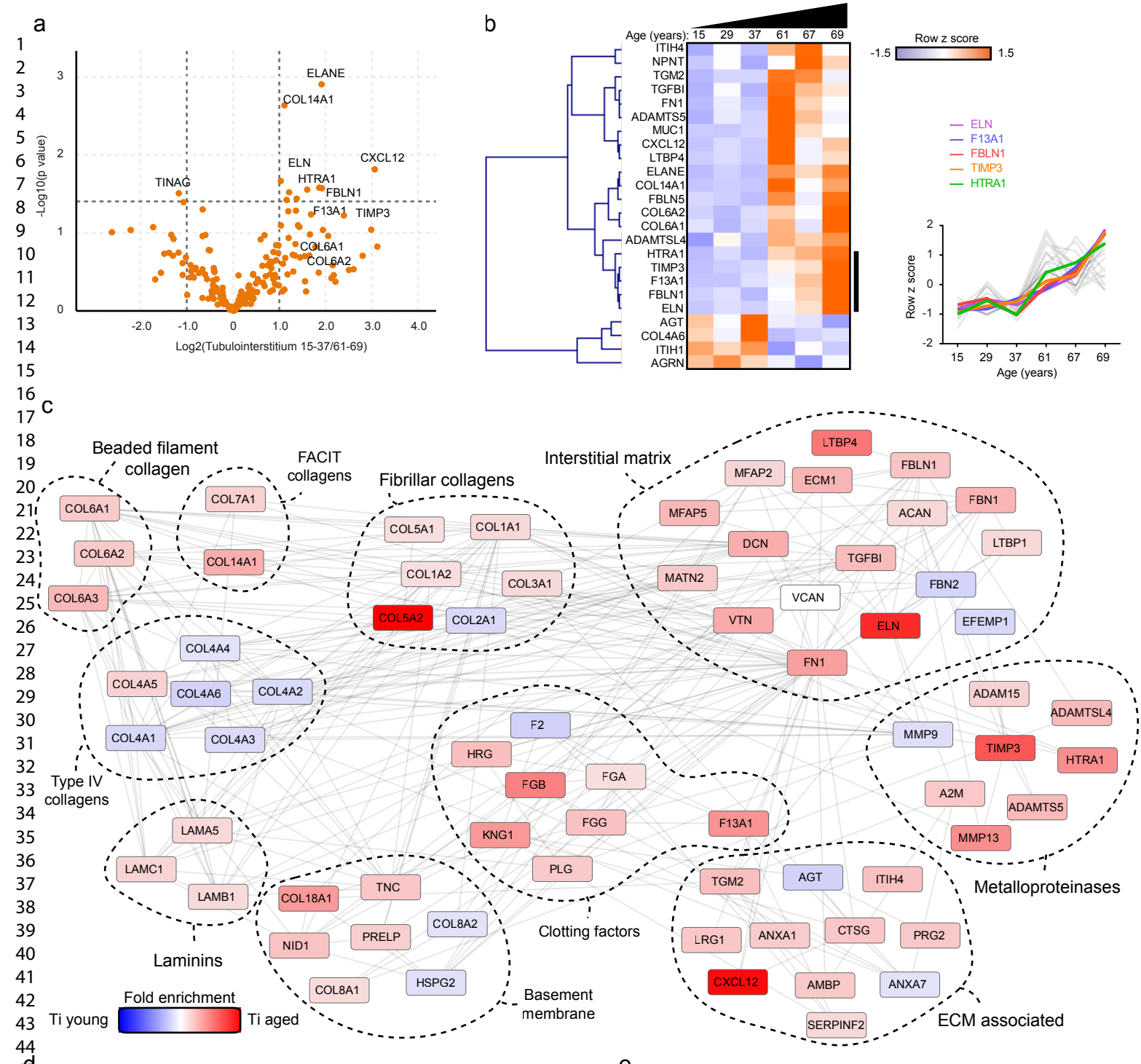

Figure 7

a

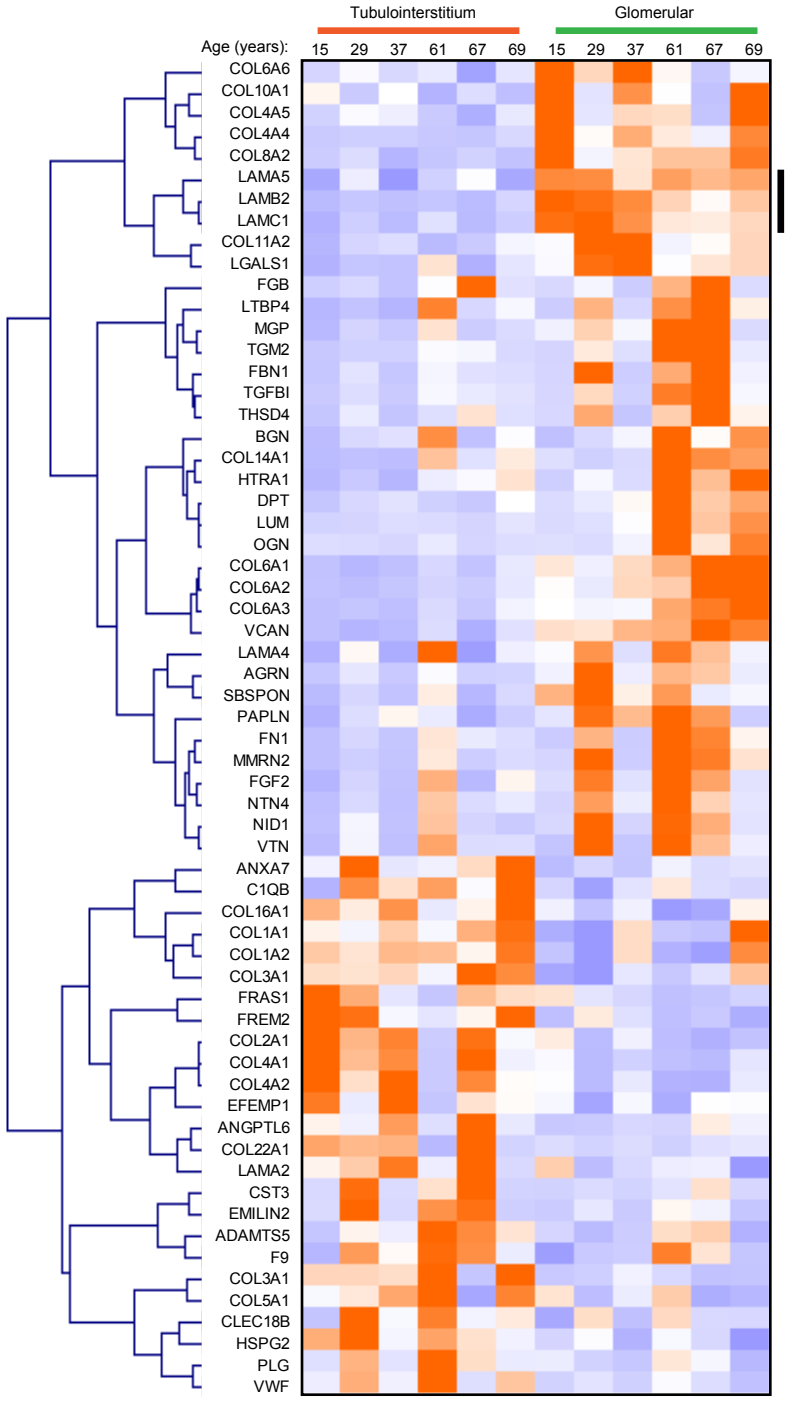

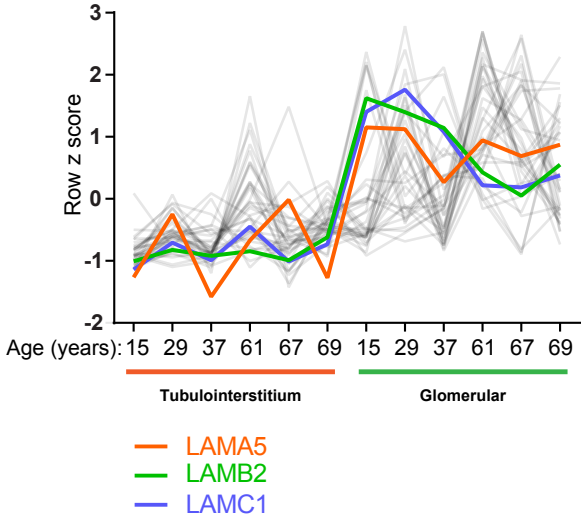

b

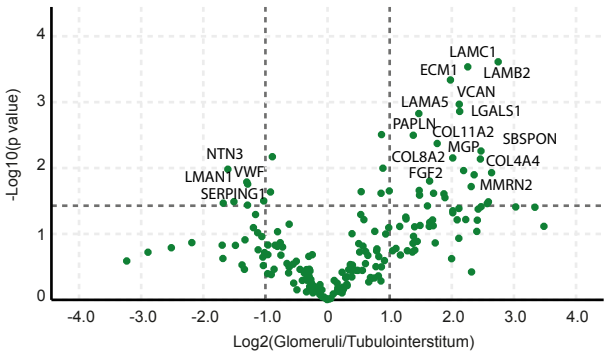

c

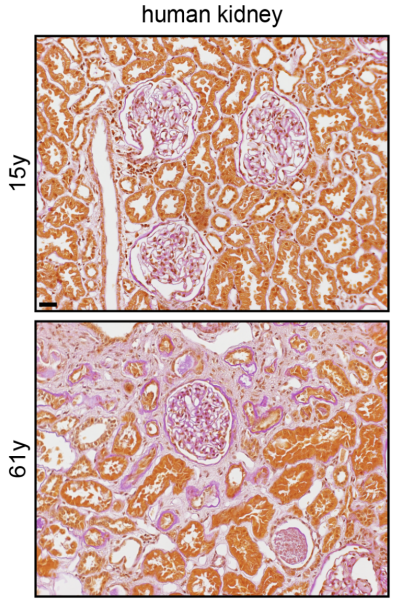

d

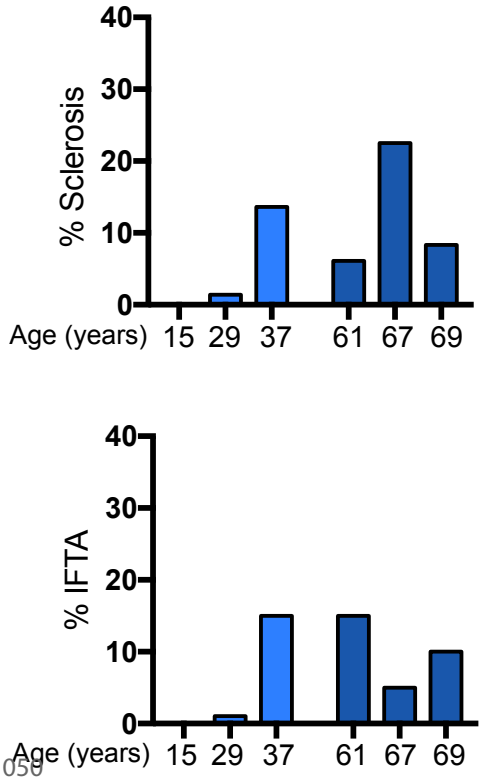

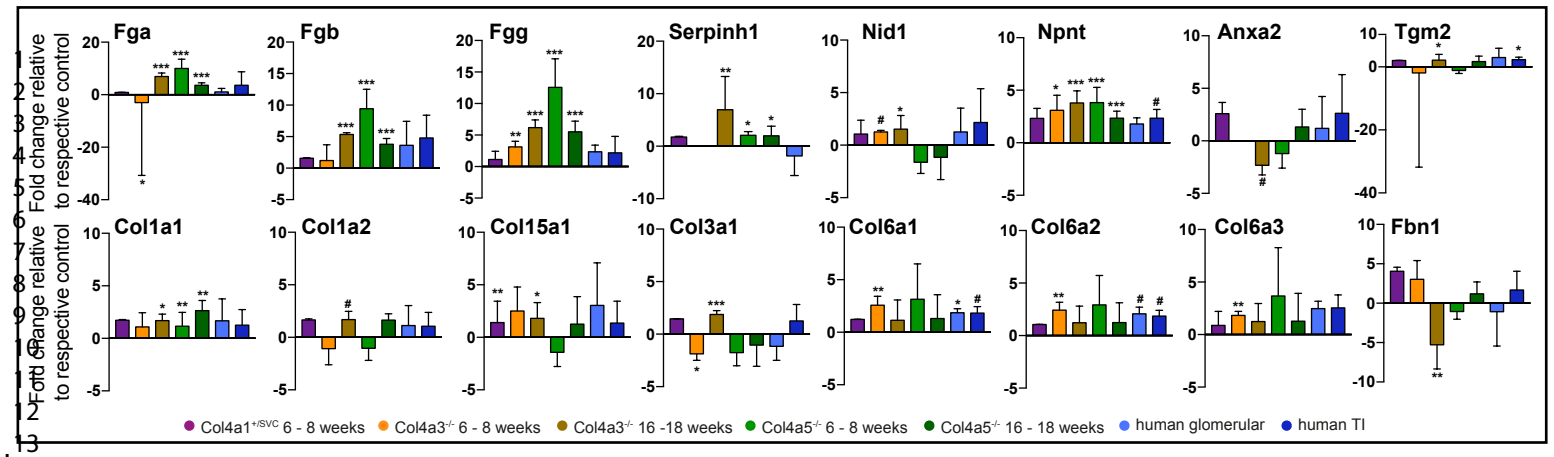
a
Fga
Fgb
Fgg
Serpinh1
Nid1
Npnt
Anxa2
Tgm2
Col1a1
Col1a2
Col15a1
Col3a1
Col6a1
Col6a2
Col6a3
Fbn1
Fold change relative to respective control
Col4a1+/SVC 6 - 8 weeks
Col4a3-/- 6 - 8 weeks
Col4a3-/- 16 -18 weeks
Col4a5-/- 6 - 8 weeks
Col4a5-/- 16 - 18 weeks
human glomerular
human TI

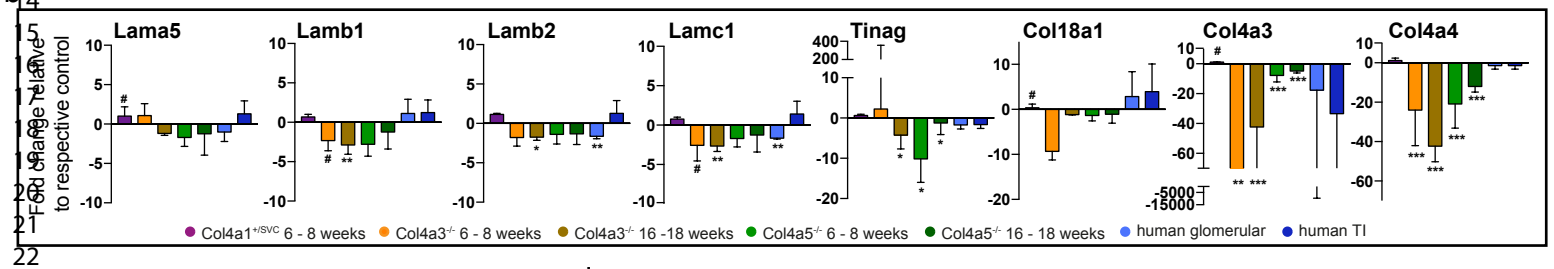
b
Lama5
Lamb1
Lamb2
Lamc1
Tinag
Col18a1
Col4a3
Col4a4
Fold change relative to respective control
Col4a1+/SVC 6 - 8 weeks
Col4a3-/- 6 - 8 weeks
Col4a3-/- 16 -18 weeks
Col4a5-/- 6 - 8 weeks
Col4a5-/- 16 - 18 weeks
human glomerular
human TI

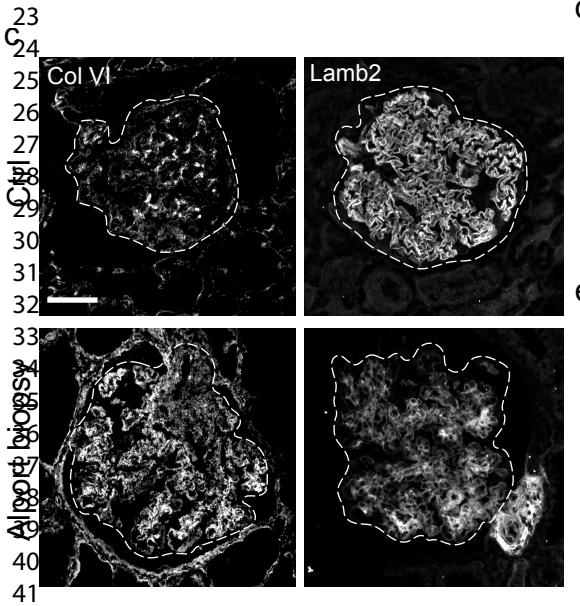
c
Col VI
Lamb2
Ctrl
Alport

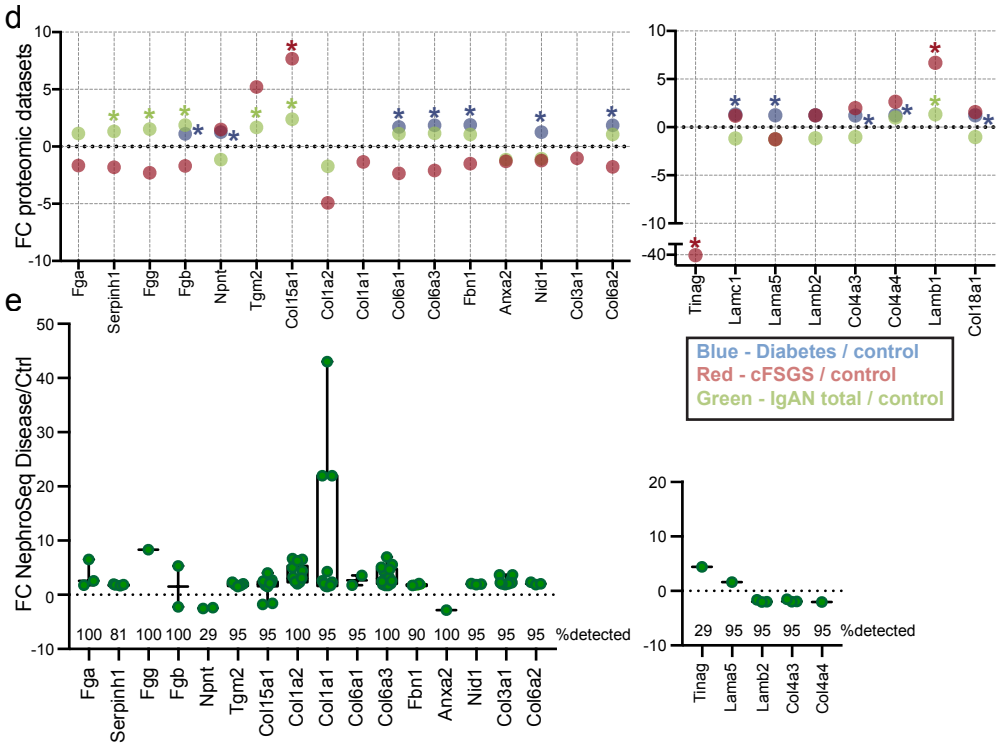
d
FC proteomic datasets
Fga
Serpinh1
Fgg
Fgb
Npnt
Tgm2
Col15a1
Col1a2
Col1a1
Col6a1
Col6a3
Fbn1
Anxa2
Nid1
Col3a1
Col6a2
Tinag
Lamc1
Lama5
Lamb2
Col4a3
Col4a4
Lamb1
Col18a1
Blue - Diabetes / control
Red - cFSGS / control
Green - IgAN total / control
e
FC NephroSeq Disease/Ctrl
100 81 100 100 29 95 95 100 95 95 100 90 100 95 95 95 %detected
29 95 95 95 95 %detected

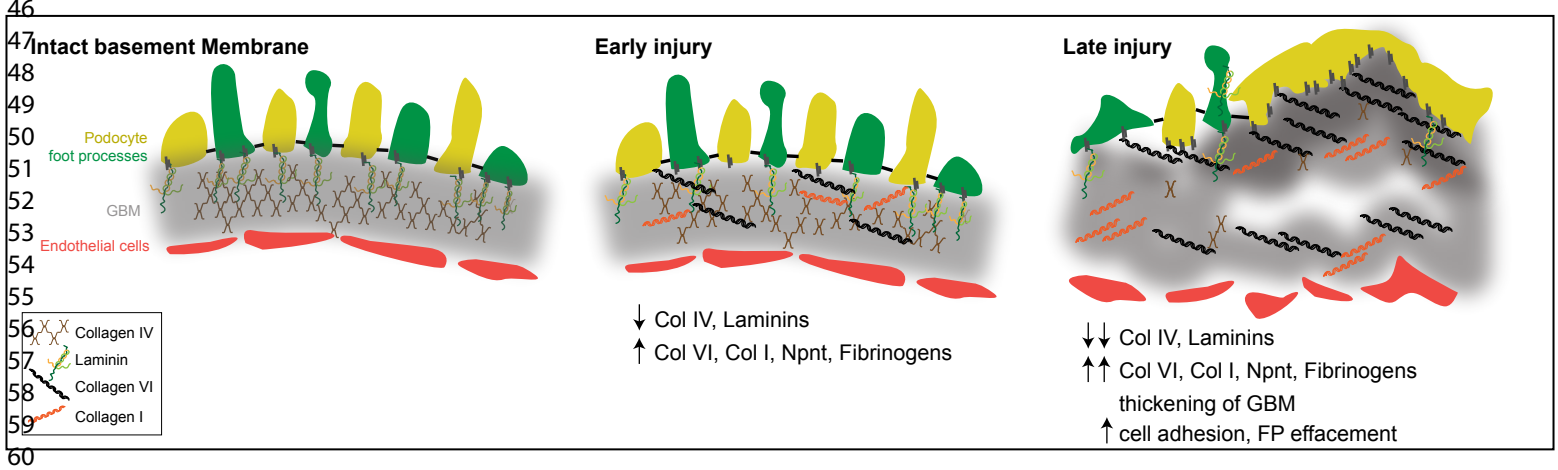
f
Intact basement Membrane
Podocyte foot processes
GBM
Endothelial cells
Collagen IV
Laminin
Collagen VI
Collagen I
Early injury
↓ Col IV, Laminins
↑ Col VI, Col I, Npnt, Fibrinogens
Late injury
↓↓ Col IV, Laminins
↑↑ Col VI, Col I, Npnt, Fibrinogens
thickening of GBM
↑ cell adhesion, FP effacement

Supplemental material

Identification of an altered matrix signature in kidney ageing and disease

*Michael J Randles[1#], *Franziska Lausecker[1], Qingyang Kong[2], Hani Suleiman[3], Graeme Reid[4], Maria Kolatsi-Joannou[5], Bernard Davenport[1], Pinyuan Tian[1], Sara Falcone[6], Paul Potter[7], Tom Van Agtmael[8], Jill T Norman[2], David A Long[5], Martin J Humphries[1], Jeffrey H Miner[3] and Rachel Lennon[1,9]

Corresponding author:
Rachel Lennon: Wellcome Centre for Cell-Matrix Research, Michael Smith Building, University of Manchester, M13 9PT, UK. Email: Rachel.Lennon@manchester.ac.uk

Table of Contents **Page**

Supplemental Videos

Video 1: SV1-Col4a1-16weeks.
Video 2: SV2-Col4a3-16weeks.
Video 3: SV3-Col4a3-28weeks.
Video 4: SV4-Col4a5-16weeks.

Supplemental Tables

Table S1: Abundance of matrix proteins in mouse models.

Table S2: Abundance of matrix proteins in human kidney.

Table S3: Human disease comparison.

Table S4: Nephroseq v5 analysis.

Table S5: Normalized abundance for all primary datasets.

Figure S1: Glomerular localization type IV collagen isoforms. Wildtype mouse cryosections were stained for the different type IV collagen alpha chains (1-6) and the podocyte marker podocin. Col4a1 and Col4a2 localise to the glomerulus, specifically to the glomerular basement membrane and Bowman's capsule basement membrane. Col4a3 and Col4a4 were detected in the GBM. Col4a5 was detected in the GBM and Bowman's capsule. Col4a6 localized to Bowman's capsule. Scale bar is 40 µm.

Figure S2: Characterisation of *Col4a5*$^{-/-}$ mice. (a) Cryosections of *Col4a5*$^{-/-}$ and *WT* mice were immunolabeled for Col4a5 and the podocyte marker podocin. Scale bar is 40 µm. (b) Albumin and creatinine concentration was measured in urine from *Col4a5*$^{-/-}$ and *WT* mice and albumin-creatinine ratios were calculated. N=5 mice per group. (c) Paraffin sections from *Col4a5*$^{-/-}$ and wild type mice were prepared and H&E stained or (d) Picro Sirius Red staining was performed. Right panel shows Picro Sirius stains exposed to polarised light. White arrowhead highlights organised collagen fibers in Bowman's capsule. Scale bar is 40 µm. (e) Percentage glomerulosclerosis and interstitial fibrosis and tubular atrophy (IFTA) was scored by a kidney pathologist. Between 62 and 118 glomeruli were examined per mouse. Pooled data from n=3 wild type mice and n=4 *Col4a5*$^{-/-}$ mice are shown. (f) Kidney samples from *Col4a5*$^{-/-}$ and wild type mice were fixed and transmission electron microscopy (TEM) performed. Yellow arrowhead highlights an area of thickened basement membrane. (g) Quantification of (f). Number of foot processes per length of GBM was calculated. GBM thickness was measured from TEM images. Pooled data from n= 3 mice per group.

Figure S3: Overview of glomerular proteomic data. (a) Gene Ontology enrichment map analysis of all proteins detected by mass spectrometry with altered abundance (>1.4 fold; p<0.1) in *Col4a1*$^{+/svc}$, *Col4a3*$^{-/-}$, *Col4a5*$^{-/-}$ mice at all analysed ages compared with aged, matched control mice. Overrepresented biological process terms are presented as nodes. (b) Comparison of wild type mice at 6-8 weeks and 16-18 weeks of age. Mass spectrometry data from matrix enriched protein fractions were filtered for known matrisome proteins. These proteins were mapped onto a merged human, mouse and rat interactome and a protein-

protein interaction network of altered mouse matrisome proteins is shown. Nodes represent proteins and edges represent reported protein-protein interactions. Colour represents fold enrichment to datasets, with increased abundance in 16-18 week wild type mice in red and increased abundance in 6-8 week old wild type mice illustrated in blue. Proteins are grouped by function.

Figure S4: Altered matrisome proteins. (a) Selected profiles of matrix proteins detected with significantly altered protein abundance in *Col4a1*$^{+/svc}$ and young *Col4a3*$^{-/-}$ and *Col4a5*$^{-/-}$ mouse glomeruli by mass spectrometry. Data are presented as log10 fold change dot plots with the mean and standard deviation shown. (d) Immunofluorescence staining for Col4a1, Col4a2, Col4a3 and Col4a4 protein in both *Col4a5*$^{-/-}$ and *WT* mice. Scale bar is 70 μm.

Figure S5: Altered matrisome proteins in *Col4a3*$^{-/-}$ mice. (a,b) Mass spectrometry data from matrix enriched protein fractions were filtered for known matrisome proteins. These proteins were mapped onto a merged human, mouse and rat interactome. Nodes represent proteins and edges represent reported protein-protein interactions. Colour represents fold enrichment to datasets, with increased abundance in *Col4a3*$^{-/-}$ relative to control illustrated in red and decreased abundance in *Col4a3*$^{-/-}$ relative to control illustrated in blue. Proteins are grouped functionally. (a) Early time point, (b) late time point.

Figure S6: Altered matrisome proteins in *Col4a5*$^{-/-}$ mice. (a,b) Mass spectrometry data from matrix enriched protein fractions were filtered for known matrisome proteins. These proteins were mapped onto a merged human, mouse and rat interactome. Nodes represent proteins and edges represent reported protein-protein interactions. Colour represents fold enrichment to datasets, with increased abundance in *Col4a5*$^{-/-}$ relative to control illustrated in red and decreased abundance in *Col4a5*$^{-/-}$ relative to control illustrated in blue. Proteins are grouped functionally. (a) Early time point, (b) late time point.

Figure S7: Human kidney data enrichment analysis. (a) Gene Ontology enrichment map analysis of all proteins detected by mass spectrometry with altered abundance (>1.4 fold; $p<0.1$) in aged human glomerular samples compared with young human glomerular samples. Overrepresented biological process terms are presented as nodes, colour represents Bonferroni-corrected p value, the lower the p value the more intense the node colour. Orange represents terms increased with age and blue represents terms decreased with age. Edge weight represents overlap between the proteins in the connected nodes. (b) Gene Ontology enrichment map analysis of all proteins detected by mass spectrometry with altered abundance (>1.4 fold; $p<0.1$) in aged tubulointerstitial samples compared with young

tubulointerstitial samples. Overrepresented biological process terms are presented as nodes. Orange represents terms increased with age and blue represents terms decreased with age.

Figure S8: Defining the tubulointerstitial matrisome. Tubulointerstitial matrix was isolated from human kidney samples and subjected analyzed by mass spectrometry. (a) Mass spectrometry data from matrix enriched protein fractions were filtered for known matrisome proteins. These proteins were mapped onto a merged human, mouse and rat interactome. Protein-protein interaction network of human tubulointerstitial matrix proteins. (b) Principal component analysis of tubulointerstitial matrix mass spectrometry data. (c) Interaction network demonstrating enrichment of matrix proteins to either glomerular (green) or tubulointerstitial (orange) compartments. Dashed lines represent interactions, nodes represent proteins. Node size relates to connectivity within the network.

Figure S9: Identification of new tubulointerstitial matrix proteins. (a) Immunofluorescence of human kidney sections for Col4a1-6 (green). DAPI stain was used to highlight nuclei. Scale bar is 50 μm. (b) Percentage of TI matrix proteins identified in the Human Protein Atlas database and their localization to different kidney compartments. (c) Venn diagram classifying the identified TI matrix proteins into different groups according to their localisation to the tubulointerstitium, tubular basement membrane (TBM), glomerular matrix (mesangium, glomerular basement membrane and Bowman's capsule basement membrane) and blood vessel matrix in the Human Protein Atlas database.

Figure S10: Defining the human kidney extracellular matrix. Mass spectrometry data from matrix enriched protein fractions were filtered for known matrisome proteins. These proteins were mapped onto a merged human, mouse and rat interactome. Protein-protein interaction network shows combined tubulointerstitial and glomerular matrix fractions colour coded and grouped based on category of matrisome protein.

Figure S11: One-hop interactors of the upregulated matrix signature proteins. Gene ontology enrichment analysis was performed on the proteins that directly interact with the identified up regulated matrix signature proteins. Three clusters were identified and the enriched terms presented as bar charts with Benjamini significance presented on the x axis.

Supplemental Videos

Video 1: SV1-Col4a1-16weeks. Serial block face-scanning electron microscopy was performed on a *Col4a1*$^{+/SVC}$ mouse (16 weeks) kidney sample and 3 dimensional ultrastructure of the glomerular filtration barrier was reconstructed using imod software. Glomerular BM is

shown in yellow, podocyte cell body in light blue, nuclei of parietal epithelial cells are shown in pink and bowman's capsule basement membrane is shown in green.

Video 2: SV2-Col4a3-16weeks. Serial block face-scanning electron microscopy was performed on a *Col4a3*$^{-/-}$ mouse (16 weeks) kidney sample and 3 dimensional ultrastructure of the glomerular filtration barrier was reconstructed using imod software. Glomerular BM is shown in yellow, podocyte cell body in light blue, bowman's capsule basement membrane is shown in green, thickness of Bowman's capsule is highlighted through dark blue lines.

Video 3: SV3-Col4a3-28weeks. Serial block face-scanning electron microscopy was performed on a *Col4a3*$^{-/-}$ mouse (28 weeks) kidney sample and 3 dimensional ultrastructure of the glomerular filtration barrier was reconstructed using imod software. Glomerular BM is shown in yellow, podocyte cell body in light blue, bowman's capsule basement membrane is shown in green and dark blue lines highlight thickened Bowman's capsule.

Video 4: SV4-Col4a5-16weeks. Serial block face-scanning electron microscopy was performed on a *Col4a5*$^{-/-}$ mouse (16 weeks) kidney sample and 3 dimensional ultrastructure of the glomerular filtration barrier was reconstructed using imod software. Glomerular BM is shown in yellow, podocyte cell body in light blue, bowman's capsule basement membrane is shown in green and the thickness of Bowman's capsule is highlighted through dark blue lines.

Supplemental Tables

Table S1. Abundance of matrix proteins identified and quantified using Progenesis were categorised as either basement membrane, other structural or ECM associated. A: *Col4a1*$^{+/svc}$, B: *Col4a3-/-* (young and adult), C: *Col4a5-/-* (young and adult). Progenesis was used to quantify proteins with the Hi-N setting, the three most abundant peptides were used for protein quantification. Anova (p) was extracted from Progenesis.

Table S2. Abundance of matrix proteins identified and quantified using Progenesis were categorised as either basement membrane, other structural or ECM associated. A: human glomerular matrix (G) and B: human tubulointerstitial matrix (T) at a range of ages (15, 29, 37, 61, 67 and 69 years).

Table S3. Signature matrix proteins were searched for their fold change gene expression levels of indicated disease datasets over control tissue samples. Data from the indicated datasets were extracted at a fold change of +/- 1.5 and $p<0.05$.

Table S4. Nephroseq v5 database was used for analysis of transcript levels of identified down regulated signature proteins.

Table S5: Normalized abundance for all primary datasets.

S1

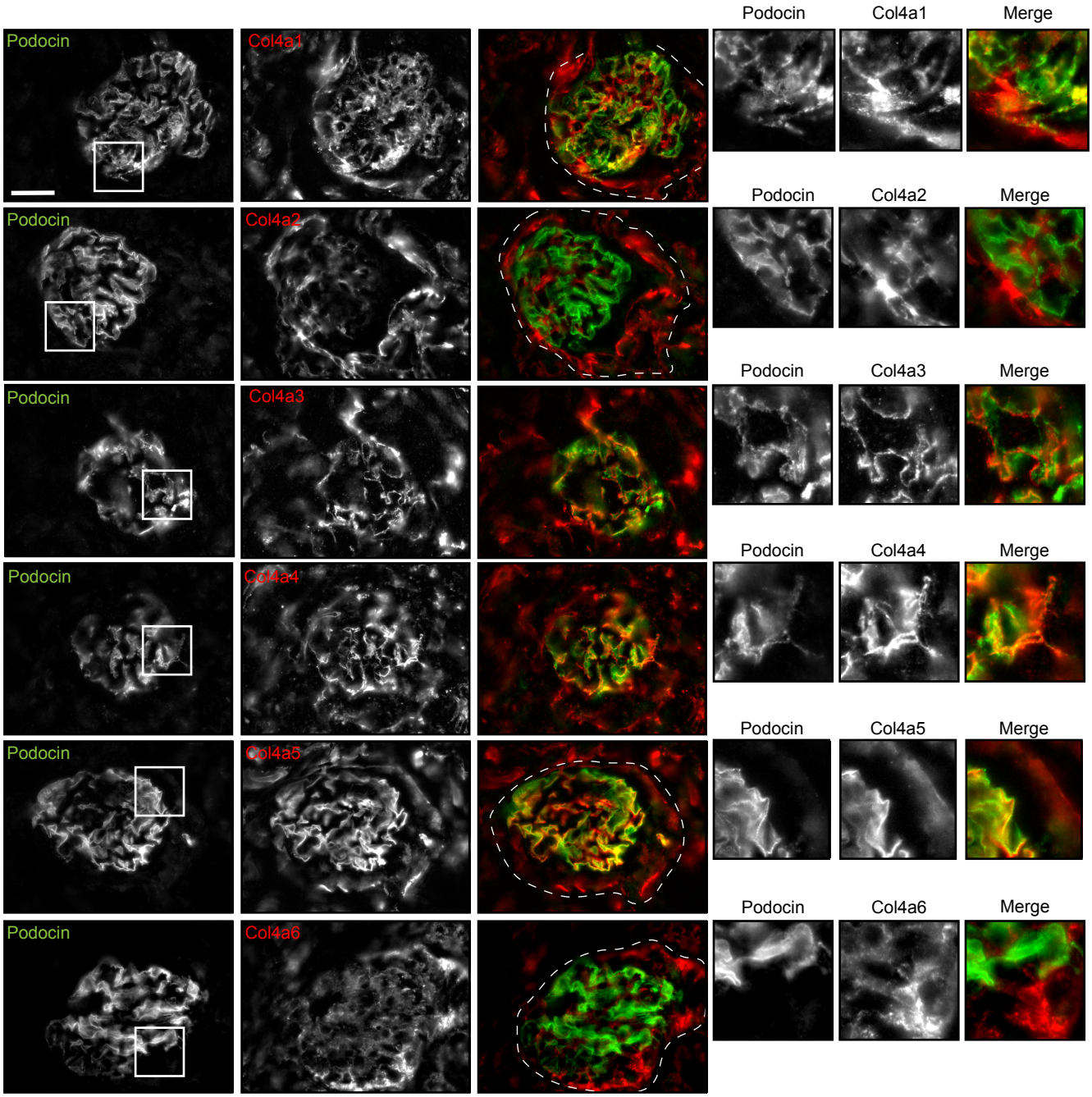
Podocin
Col4a1
Podocin
Col4a1
Merge
Podocin
Col4a2
Podocin
Col4a2
Merge
Podocin
Col4a3
Podocin
Col4a3
Merge
Podocin
Col4a4
Podocin
Col4a4
Merge
Podocin
Col4a5
Podocin
Col4a5
Merge
Podocin
Col4a6
Podocin
Col4a6
Merge

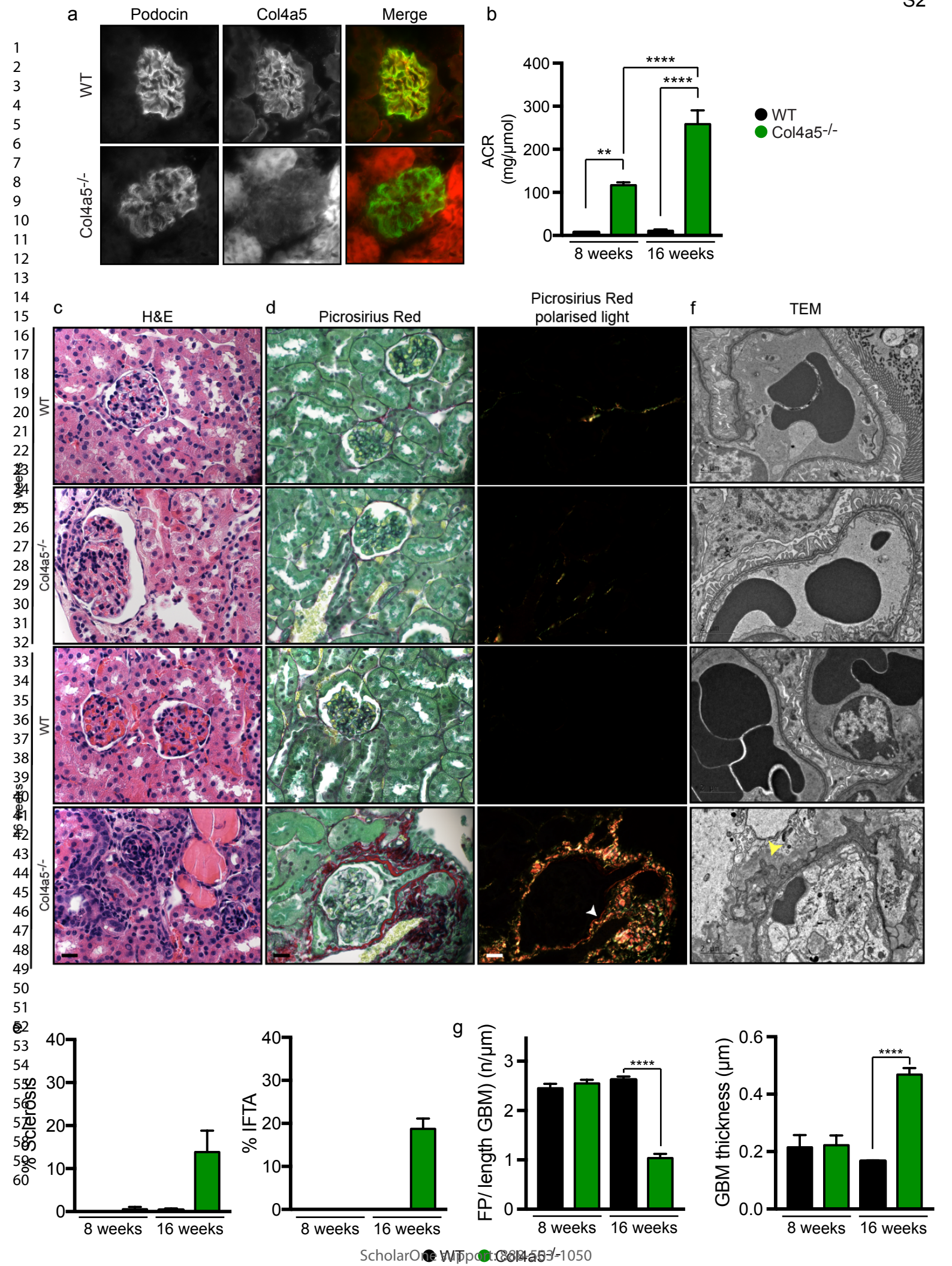

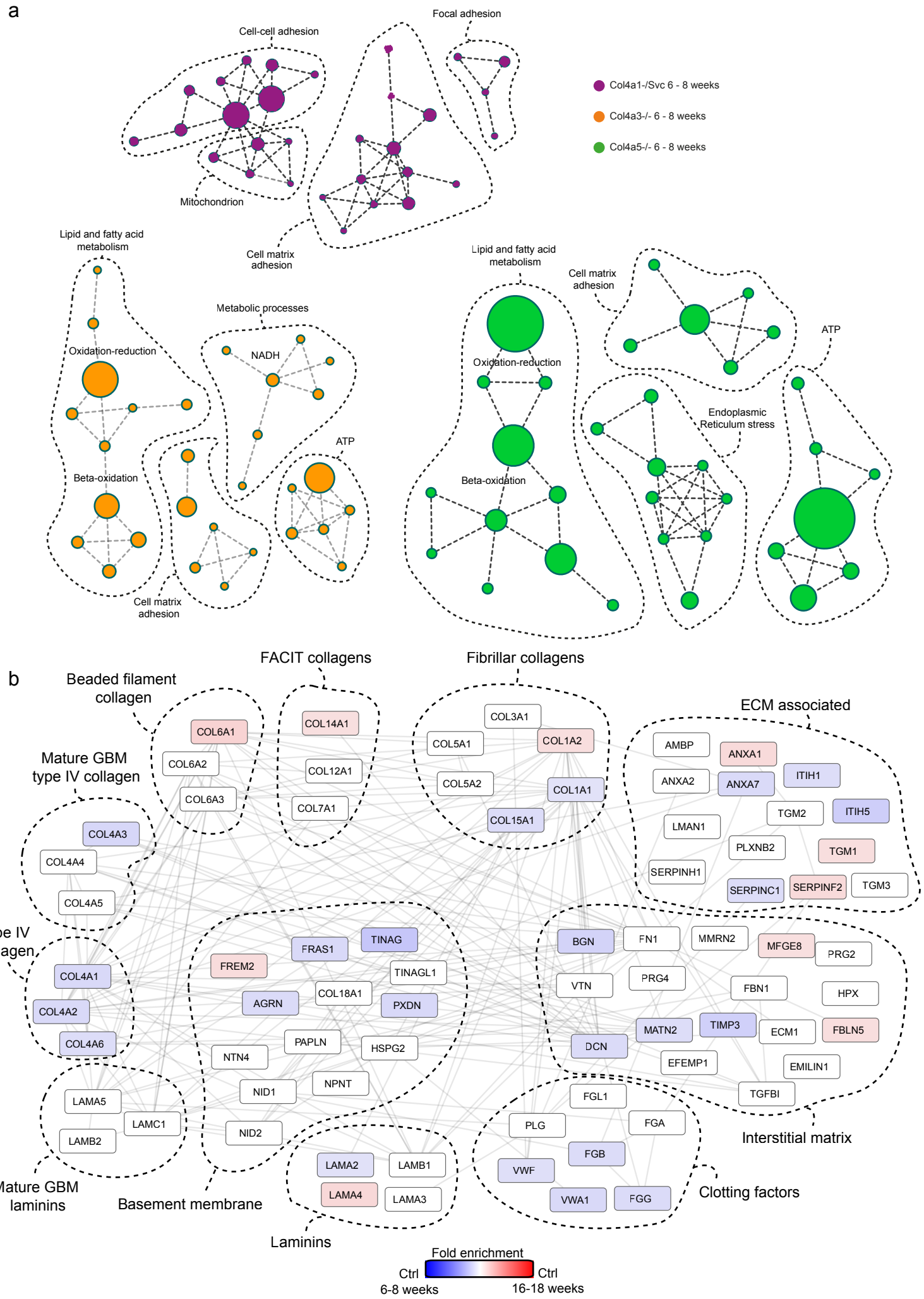
a
Cell-cell adhesion
Focal adhesion
Mitochondrion
Cell matrix adhesion
Col4a1-/Svc 6 - 8 weeks
Col4a3-/- 6 - 8 weeks
Col4a5-/- 6 - 8 weeks
Lipid and fatty acid metabolism
Metabolic processes
Oxidation-reduction
NADH
ATP
Beta-oxidation
Cell matrix adhesion
Lipid and fatty acid metabolism
Cell matrix adhesion
ATP
Oxidation-reduction
Endoplasmic Reticulum stress
Beta-oxidation
b
FACIT collagens
Fibrillar collagens
Beaded filament collagen
ECM associated
Mature GBM type IV collagen
COL6A1
COL6A2
COL6A3
COL14A1
COL12A1
COL7A1
COL3A1
COL5A1
COL1A2
COL5A2
COL1A1
COL15A1
AMBP
ANXA1
ANXA2
ANXA7
ITIH1
TGM2
ITIH5
LMAN1
PLXNB2
TGM1
SERPINH1
SERPINC1
SERPINF2
TGM3
COL4A3
COL4A4
COL4A5
Type IV collagen
COL4A1
COL4A2
COL4A6
FREM2
FRAS1
TINAG
TINAGL1
AGRN
COL18A1
PXDN
PAPLN
HSPG2
NTN4
NID1
NPNT
NID2
BGN
FN1
MMRN2
MFGE8
PRG2
VTN
PRG4
FBN1
HPX
MATN2
TIMP3
ECM1
FBLN5
DCN
EFEMP1
EMILIN1
TGFBI
Interstitial matrix
LAMA5
LAMC1
LAMB2
Mature GBM laminins
Basement membrane
LAMA2
LAMB1
LAMA4
LAMA3
Laminins
FGL1
PLG
FGA
FGB
VWF
VWA1
FGG
Clotting factors
Fold enrichment
Ctrl
6-8 weeks
Ctrl
16-18 weeks

a

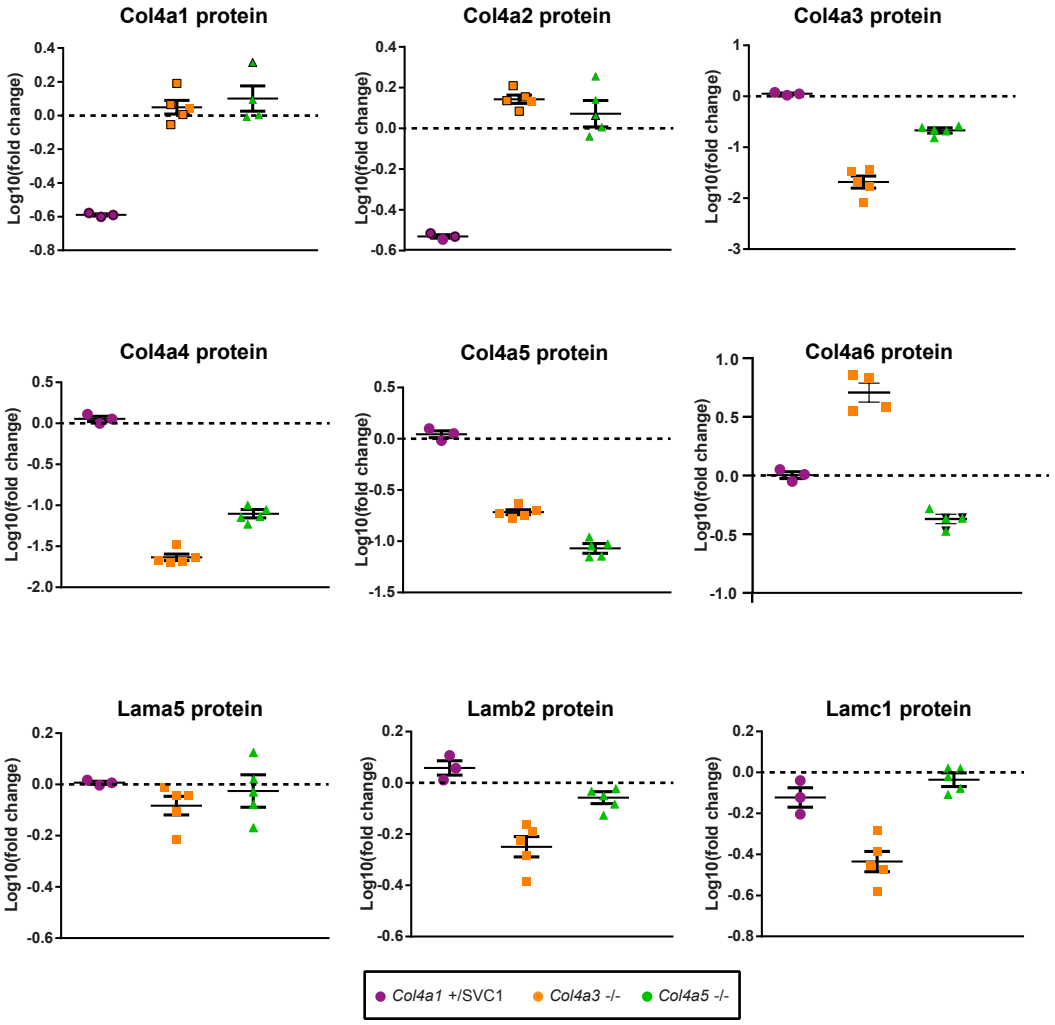
Col4a1 protein
Col4a2 protein
Col4a3 protein
Col4a4 protein
Col4a5 protein
Col4a6 protein
Lama5 protein
Lamb2 protein
Lamc1 protein
Log10(fold change)
Col4a1 +/SVC1
Col4a3 -/-
Col4a5 -/-

b

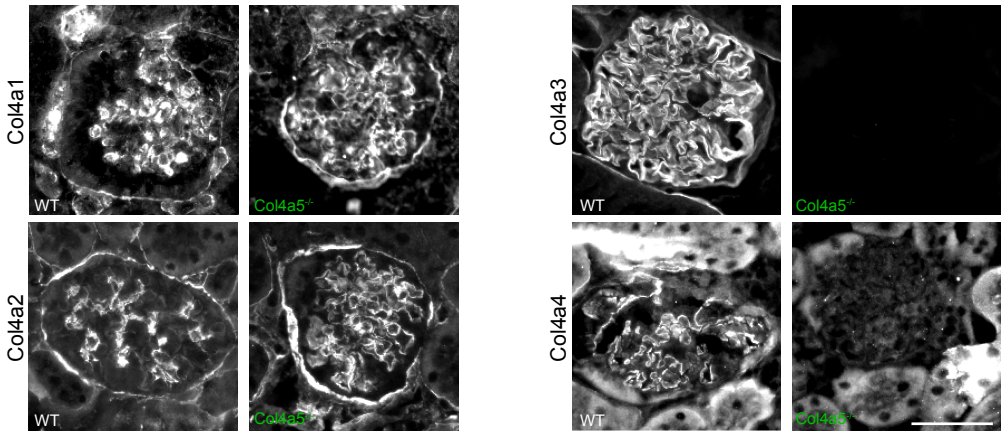
Col4a1
Col4a2
Col4a3
Col4a4
WT
Col4a5-/-

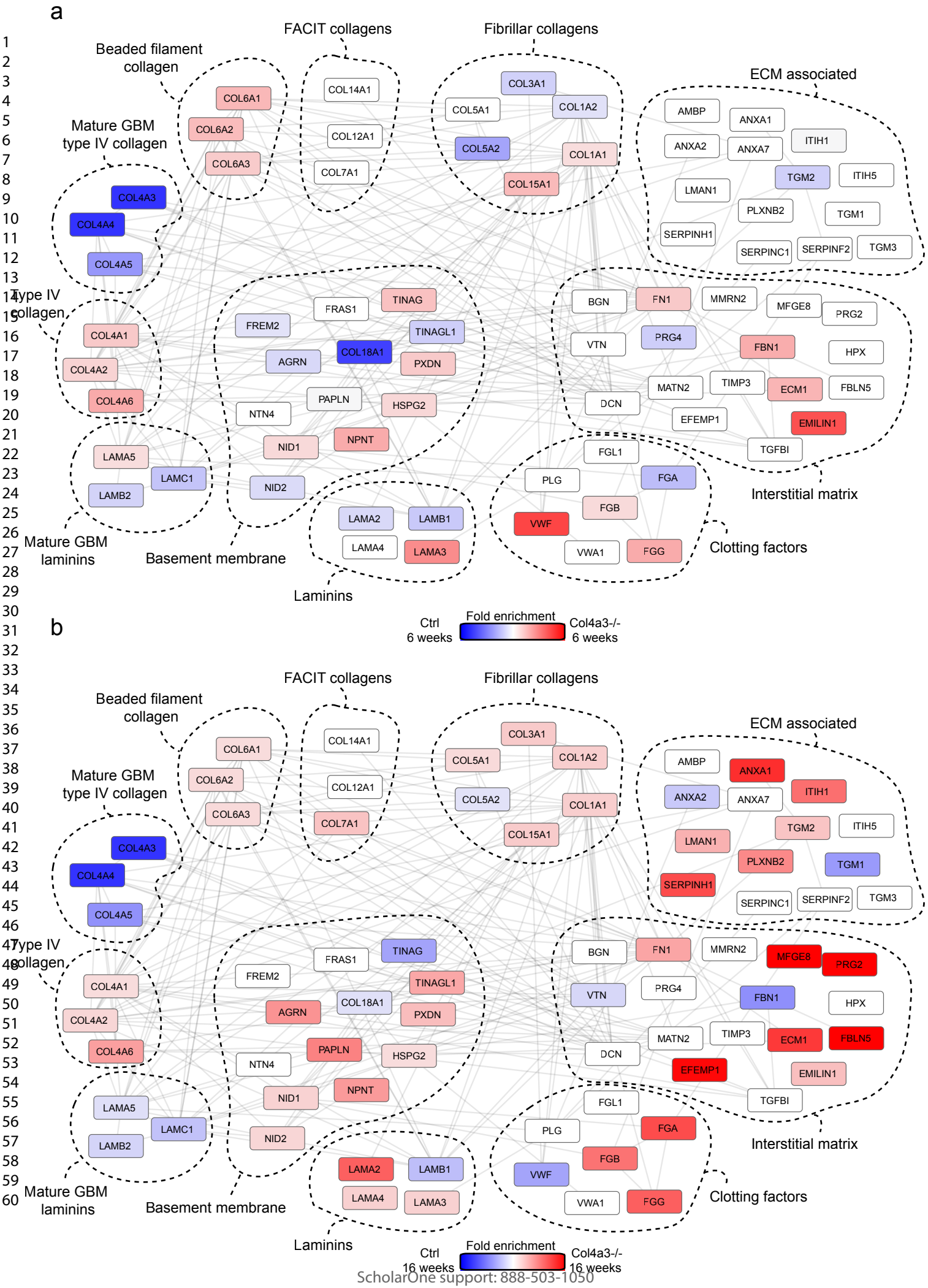

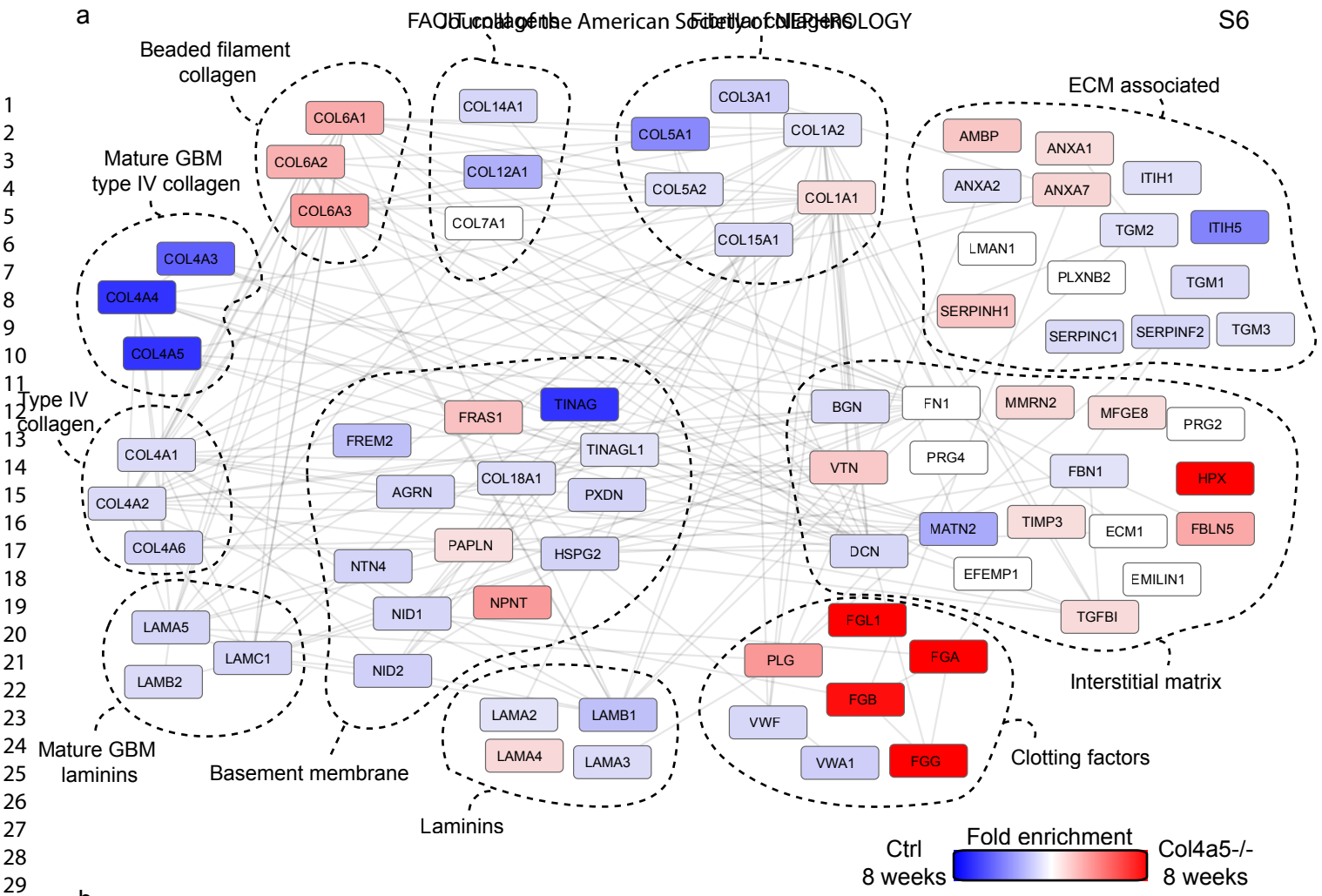
a
Beaded filament collagen
Mature GBM type IV collagen
Type IV collagen
COL6A1
COL6A2
COL6A3
COL14A1
COL12A1
COL7A1
COL3A1
COL5A1
COL1A2
COL5A2
COL1A1
COL15A1
ECM associated
AMBP
ANXA1
ANXA2
ANXA7
ITIH1
ITIH5
TGM2
TGM1
TGM3
LMAN1
PLXNB2
SERPINH1
SERPINC1
SERPINF2
COL4A3
COL4A4
COL4A5
COL4A1
COL4A2
COL4A6
FRAS1
TINAG
FREM2
TINAGL1
AGRN
COL18A1
PXDN
PAPLN
HSPG2
NTN4
NPNT
NID1
NID2
BGN
FN1
MMRN2
MFGE8
PRG2
VTN
PRG4
FBN1
HPX
MATN2
TIMP3
ECM1
FBLN5
DCN
EFEMP1
EMILIN1
TGFBI
LAMA5
LAMC1
LAMB2
LAMA2
LAMB1
LAMA4
LAMA3
FGL1
PLG
FGA
FGB
VWF
VWA1
FGG
Interstitial matrix
Clotting factors
Mature GBM laminins
Basement membrane
Laminins
Ctrl 8 weeks
Fold enrichment
Col4a5-/- 8 weeks

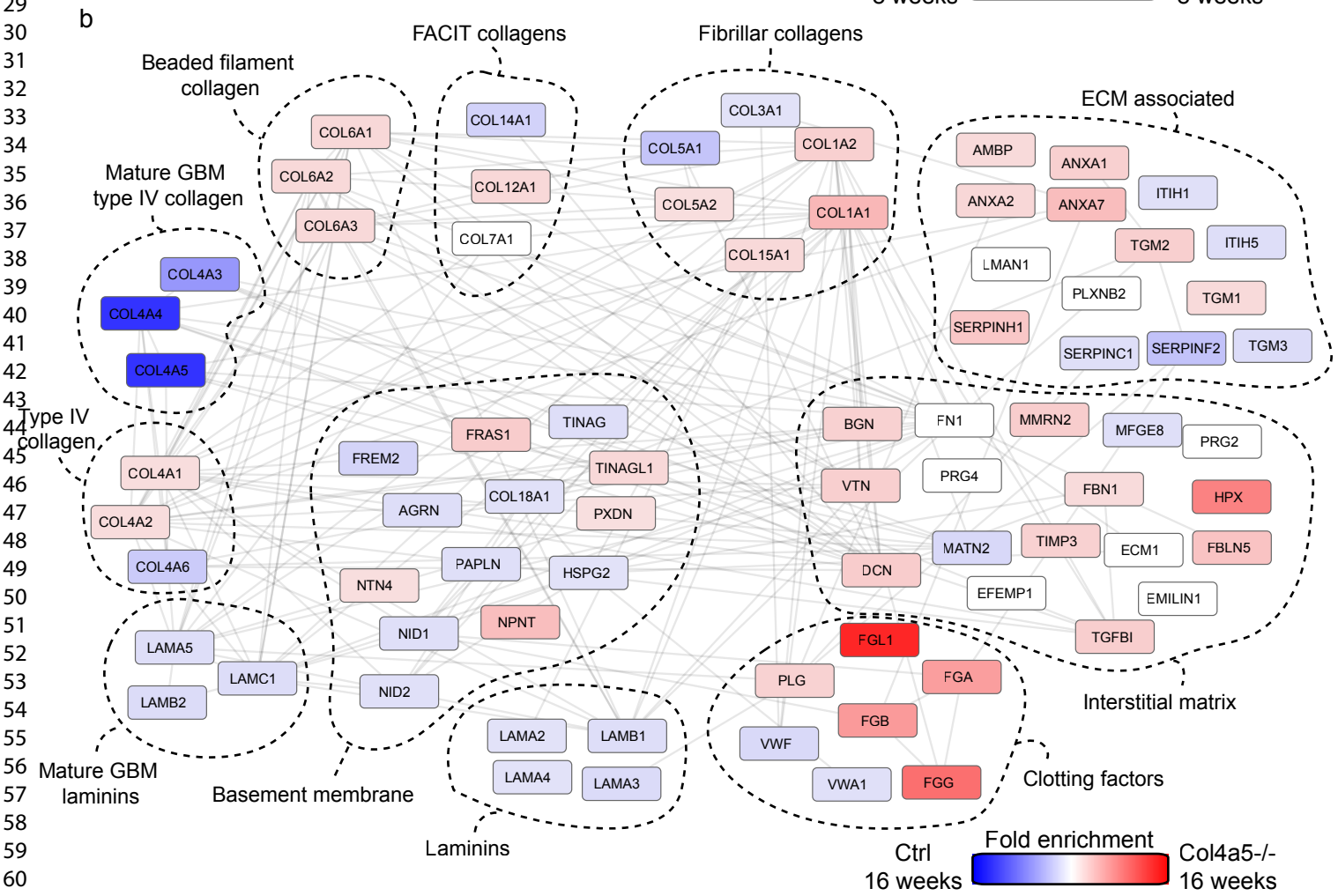
b
FACIT collagens
Fibrillar collagens
Beaded filament collagen
Mature GBM type IV collagen
Type IV collagen
COL6A1
COL6A2
COL6A3
COL14A1
COL12A1
COL7A1
COL3A1
COL5A1
COL1A2
COL5A2
COL1A1
COL15A1
ECM associated
AMBP
ANXA1
ANXA2
ANXA7
ITIH1
ITIH5
TGM2
TGM1
TGM3
LMAN1
PLXNB2
SERPINH1
SERPINC1
SERPINF2
COL4A3
COL4A4
COL4A5
COL4A1
COL4A2
COL4A6
FRAS1
TINAG
FREM2
TINAGL1
AGRN
COL18A1
PXDN
PAPLN
HSPG2
NTN4
NPNT
NID1
NID2
BGN
FN1
MMRN2
MFGE8
PRG2
VTN
PRG4
FBN1
HPX
MATN2
TIMP3
ECM1
FBLN5
DCN
EFEMP1
EMILIN1
TGFBI
LAMA5
LAMC1
LAMB2
LAMA2
LAMB1
LAMA4
LAMA3
FGL1
PLG
FGA
FGB
VWF
VWA1
FGG
Interstitial matrix
Clotting factors
Mature GBM laminins
Basement membrane
Laminins
Ctrl 16 weeks
Fold enrichment
Col4a5-/- 16 weeks

a

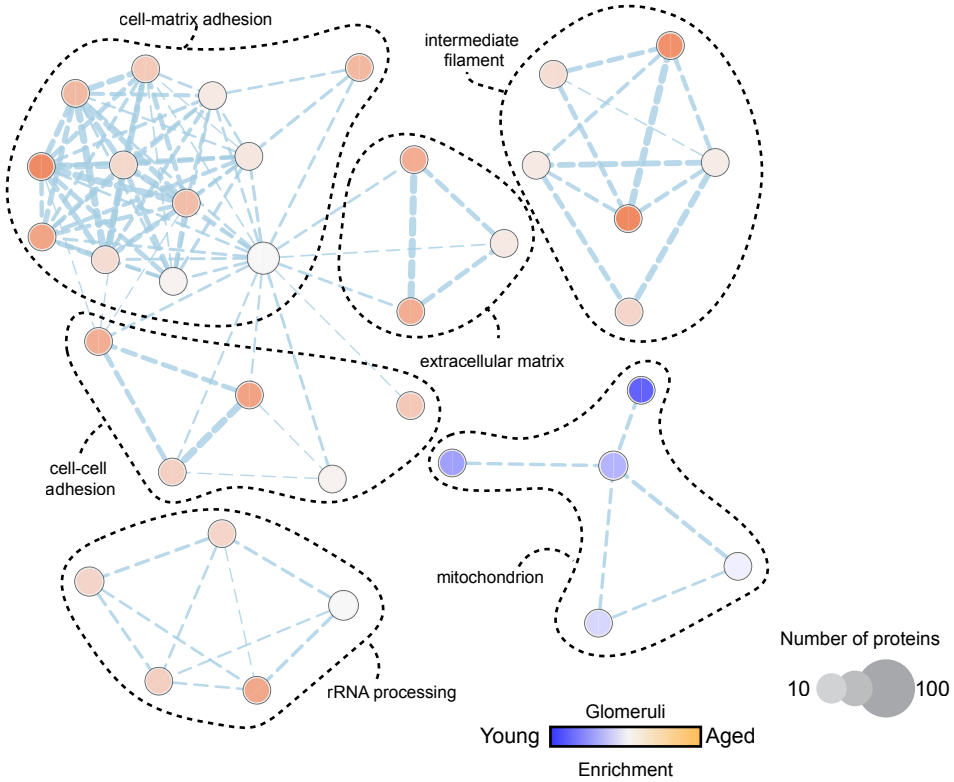
cell-matrix adhesion
intermediate filament
extracellular matrix
cell-cell adhesion
mitochondrion
rRNA processing
Number of proteins
10
100
Glomeruli
Young
Aged
Enrichment

b

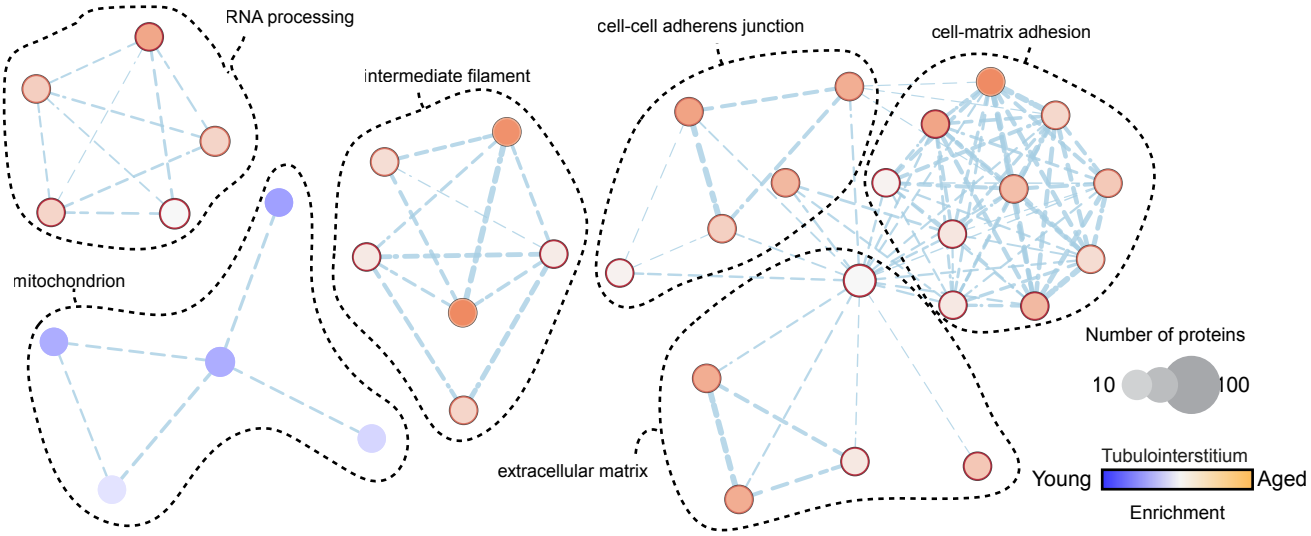
RNA processing
intermediate filament
cell-cell adherens junction
cell-matrix adhesion
mitochondrion
extracellular matrix
Number of proteins
10
100
Tubulointerstitium
Young
Aged
Enrichment

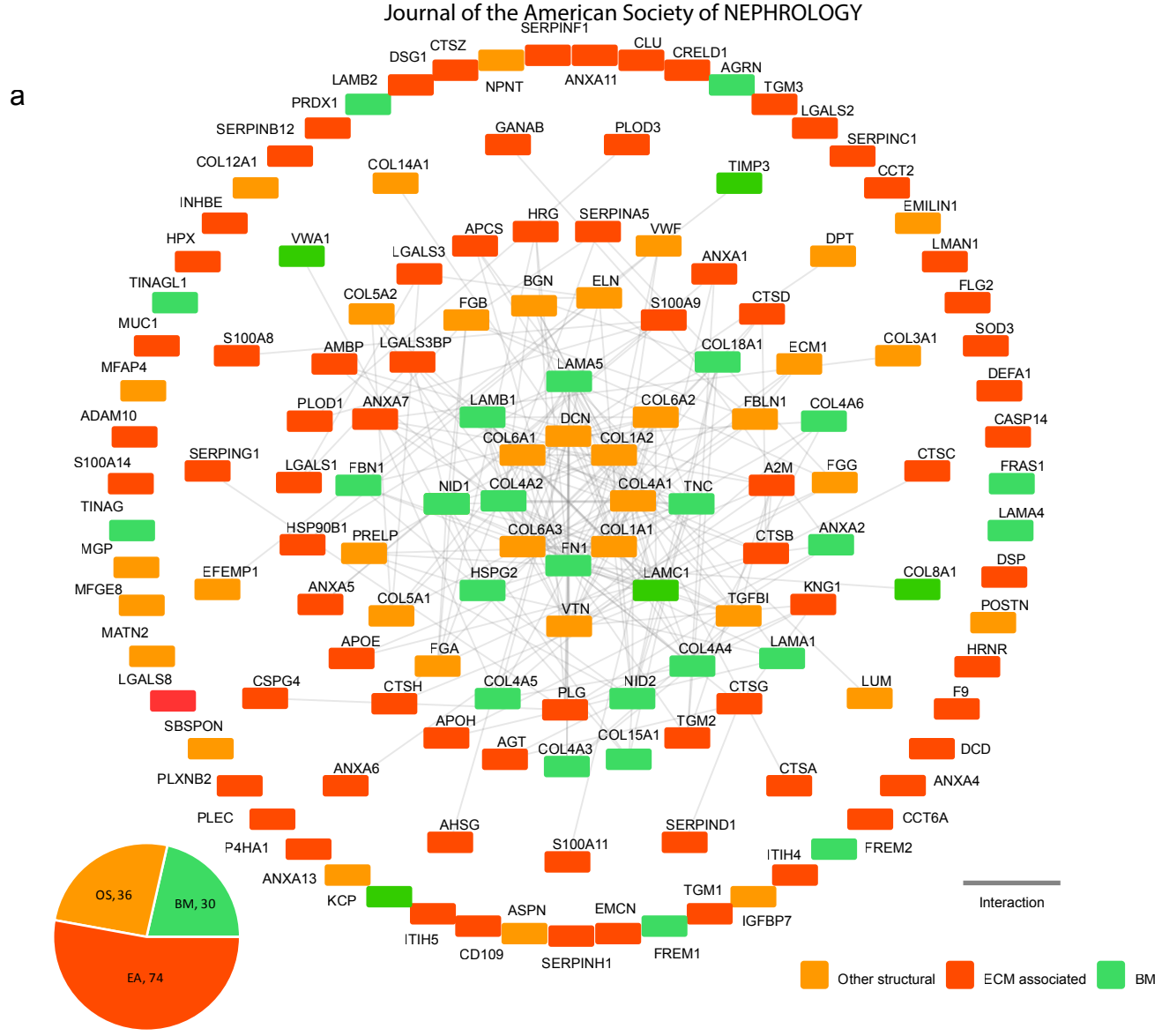
a
SERPINF1
CTSZ
DSG1
CLU
CRELD1
AGRN
LAMB2
NPNT
ANXA11
TGM3
PRDX1
LGALS2
SERPINB12
GANAB
PLOD3
SERPINC1
COL12A1
COL14A1
TIMP3
CCT2
INHBE
EMILIN1
HRG
SERPINA5
HPX
VWA1
APCS
VWF
DPT
LMAN1
LGALS3
ANXA1
TINAGL1
BGN
ELN
FLG2
COL5A2
FGB
S100A9
CTSD
MUC1
S100A8
AMBP
LGALS3BP
COL18A1
ECM1
COL3A1
SOD3
MFAP4
LAMA5
DEFA1
ADAM10
PLOD1
ANXA7
LAMB1
COL6A2
FBLN1
COL4A6
CASP14
DCN
COL6A1
COL1A2
S100A14
SERPING1
CTSC
FRAS1
LGALS1
FBN1
A2M
FGG
NID1
COL4A2
COL4A1
TNC
TINAG
LAMA4
HSP90B1
PRELP
COL6A3
COL1A1
CTSB
ANXA2
MGP
FN1
DSP
EFEMP1
HSPG2
LAMC1
COL8A1
MFGE8
ANXA5
COL5A1
KNG1
TGFBI
POSTN
VTN
MATN2
APOE
FGA
COL4A4
LAMA1
HRNR
LGALS8
CSPG4
CTSH
COL4A5
PLG
NID2
CTSG
LUM
F9
SBSPON
APOH
TGM2
AGT
COL4A3
COL15A1
DCD
PLXNB2
ANXA6
CTSA
ANXA4
PLEC
AHSG
SERPIND1
CCT6A
P4HA1
S100A11
ITIH4
FREM2
ANXA13
KCP
TGM1
IGFBP7
ITIH5
ASPN
EMCN
CD109
SERPINH1
FREM1
OS, 36
BM, 30
EA, 74
Interaction
Other structural
ECM associated
BM
b
T61
T69
T29
T37
T15
T67
aged TI samples
young TI samples
Component 2 (7%)
Component 1 (91%)
0.6
0.4
0.2
0
-0.2
-0.4
0.850
0.875
0.900
0.925
0.950
0.975
c
OGN
AGRN
MMRN2
LAMB2
SBSPON
CST3
LGALS1
EMILIN2
LUM
COL8A2
FBN1
MGP
VWF
COL4A4
FREM2
PLG
DPT
COL6A3
COL6A2
VCAN
ADAMTS5
COL4A1
LAMC1
COL11A2
ANXA7
COL4A2
COL6A1
NID1
CLEC18B
THSD4
COL3A1
TGFBI
COL2A1
TGM2
ANGPTL6
FN1
COL10A1
COL16A1
COL1A2
HTRA1
FRAS1
COL1A1
LAMA5
PAPLN
HSPG2
VTN
FGF2
F9
NTN4
COL5A1
BGN
COL4A5
FGB
EFEMP1
LTBP4
LAMA2
COL14A1
C1QB
COL6A6
COL22A1
LAMA4
Number of interactors
Tubulointerstitium
Glomerular

a

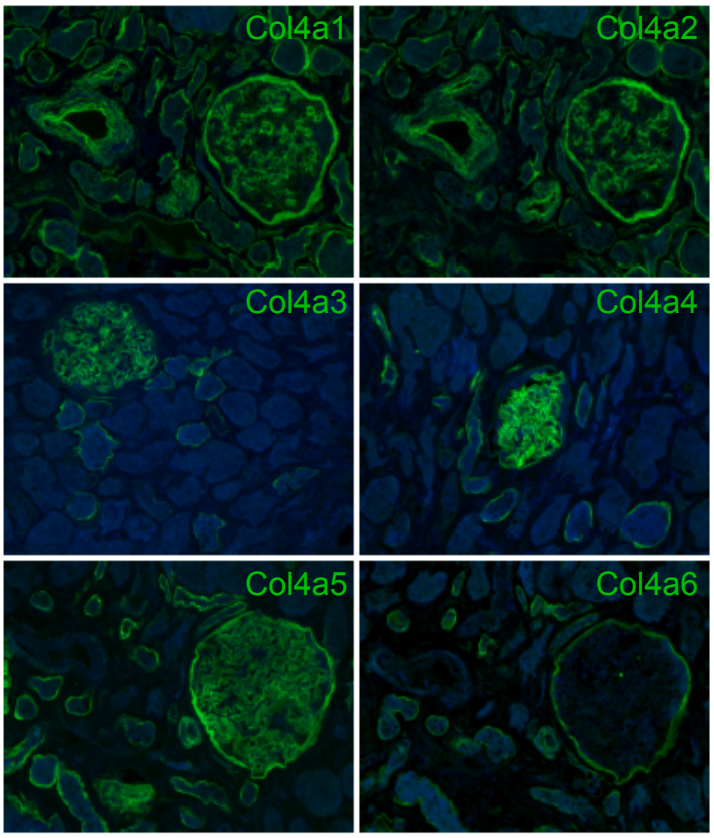
Col4a1
Cbl4a2
Col4a3
Col4a4
Col4a5
Col4a6

b

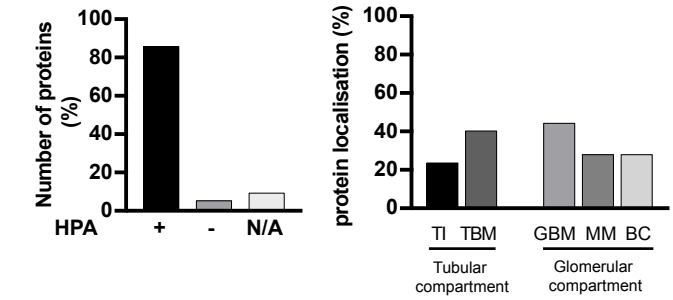
Number of proteins (%)
100
80
60
40
20
0
HPA
+
-
N/A
protein localisation (%)
100
80
60
40
20
0
TI TBM
GBM MM BC
Tubular compartment
Glomerular compartment

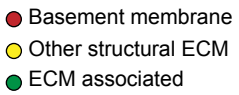
Basement membrane
Other structural ECM
ECM associated

c

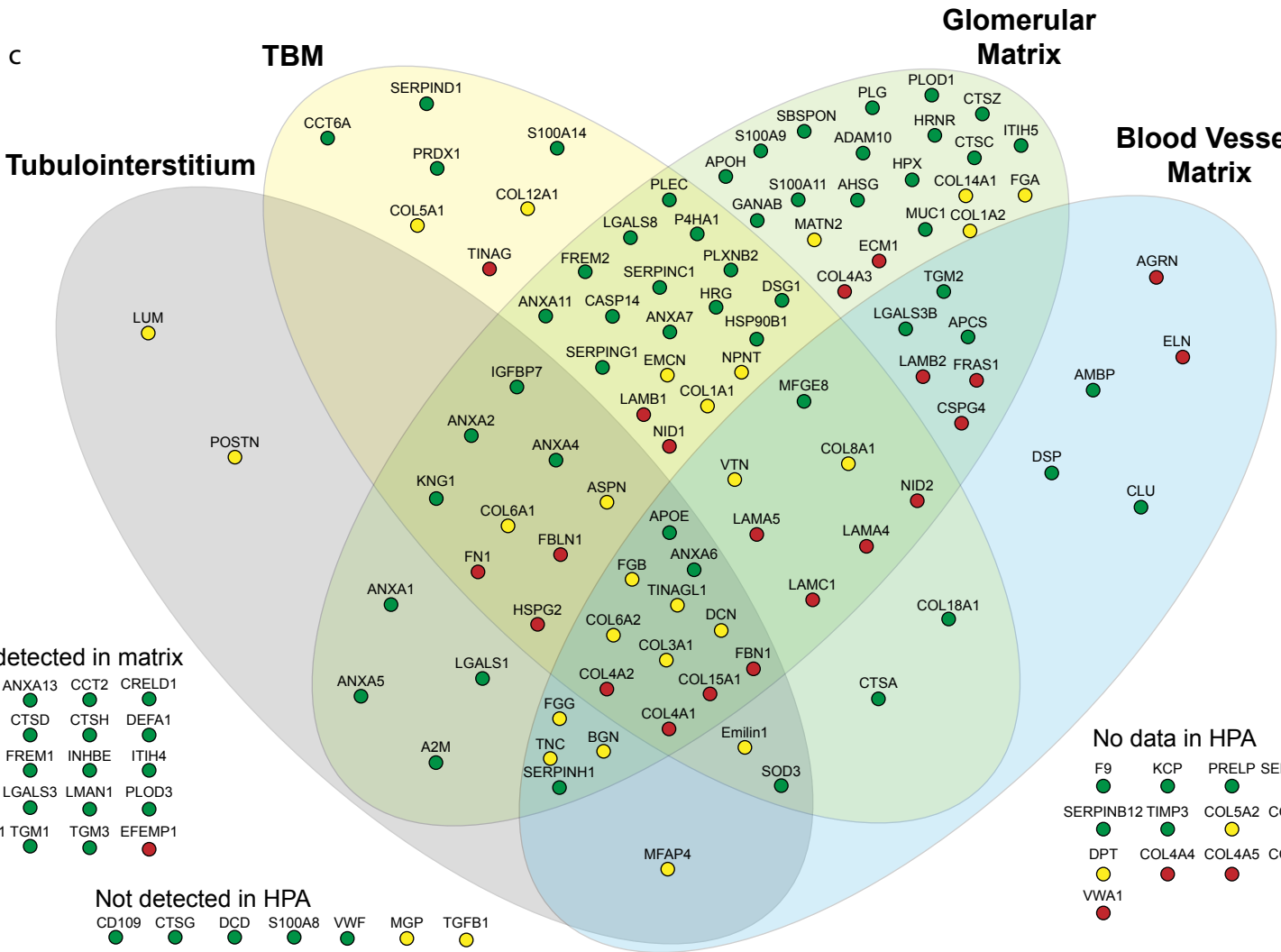
TBM
Glomerular Matrix
Tubulointerstitium
Blood Vessel Matrix
SERPIND1
CCT6A
S100A14
PRDX1
COL12A1
COL5A1
TINAG
LUM
POSTN
PLOD1
PLG
CTSZ
SBSPON
HRNR
ITIH5
S100A9
ADAM10
CTSC
APOH
HPX
PLEC
S100A11
AHSG
COL14A1
FGA
GANAB
MUC1
COL1A2
LGALS8
P4HA1
MATN2
ECM1
FREM2
PLXNB2
SERPINC1
COL4A3
TGM2
DSG1
HRG
ANXA11
CASP14
ANXA7
HSP90B1
LGALS3B
APCS
SERPING1
EMCN
NPNT
LAMB2
FRAS1
IGFBP7
MFGE8
LAMB1
COL1A1
CSPG4
ANXA2
NID1
ANXA4
COL8A1
VTN
KNG1
ASPN
NID2
COL6A1
APOE
LAMA5
FBLN1
LAMA4
FN1
ANXA6
FGB
TINAGL1
LAMC1
ANXA1
HSPG2
COL18A1
COL6A2
DCN
COL3A1
FBN1
LGALS1
ANXA5
COL4A2
COL15A1
CTSA
FGG
COL4A1
Emilin1
A2M
TNC
BGN
SERPINH1
SOD3
MFAP4
AGRN
ELN
AMBP
DSP
CLU
Not detected in matrix
AGT
ANXA13
CCT2
CRELD1
CTSB
CTSD
CTSH
DEFA1
FLG2
FREM1
INHBE
ITIH4
LGALS2
LGALS3
LMAN1
PLOD3
SERPINF1
TGM1
TGM3
EFEMP1
LAMA1
Not detected in HPA
CD109
CTSG
DCD
S100A8
VWF
MGP
TGFB1
No data in HPA
F9
KCP
PRELP
SERPINA5
SERPINB12
TIMP3
COL5A2
COL6A3
DPT
COL4A4
COL4A5
COL4A6
VWA1

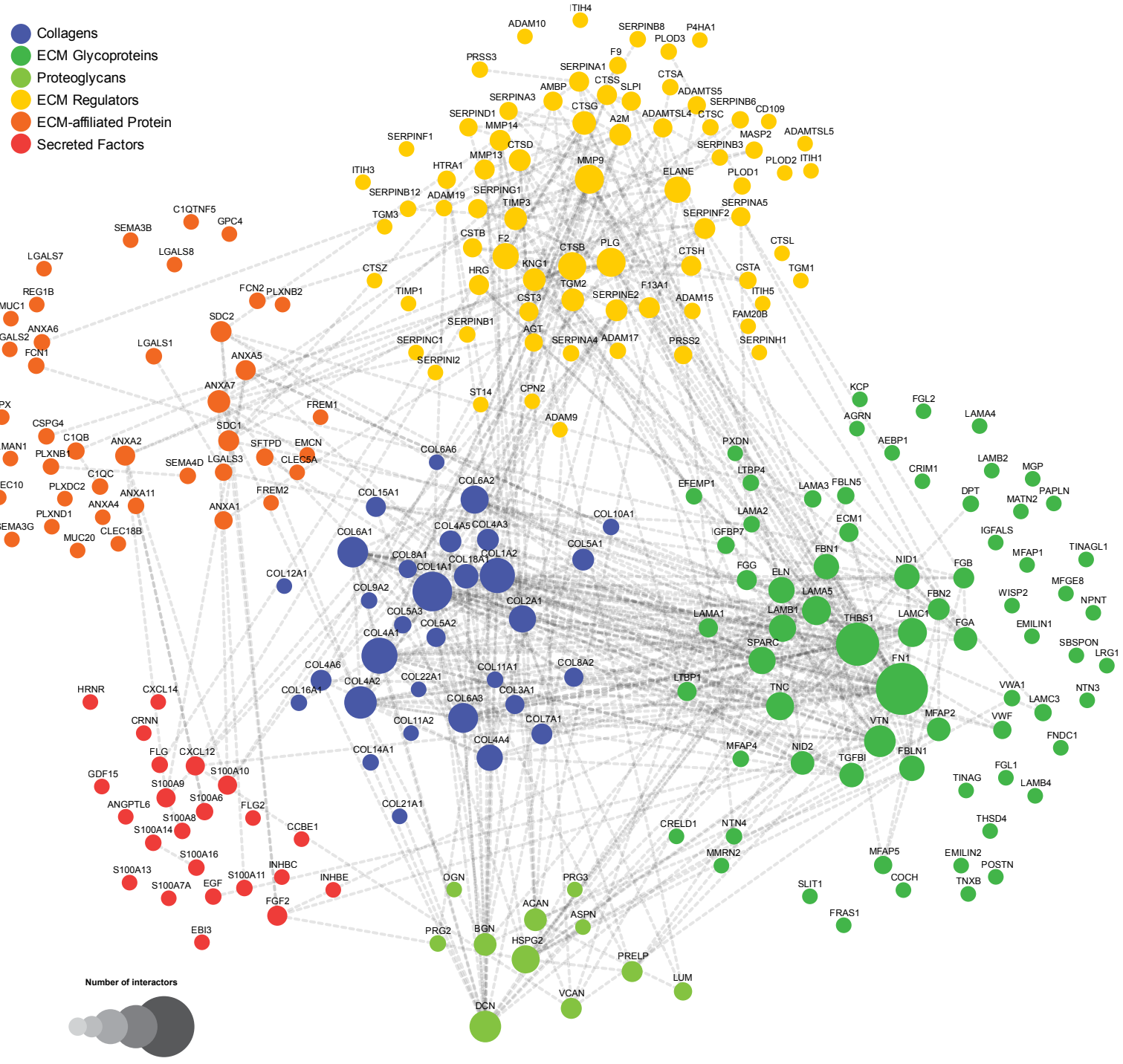
Collagens
ECM Glycoproteins
Proteoglycans
ECM Regulators
ECM-affiliated Protein
Secreted Factors
Number of interactors
ITIH4
ADAM10
SERPINB8
P4HA1
PLOD3
PRSS3
F9
SERPINA1
CTSA
AMBP
CTSS
SLPI
ADAMTS5
SERPINA3
SERPINB6
CD109
SERPIND1
CTSG
ADAMTSL4
CTSC
A2M
MMP14
MASP2
ADAMTSL5
SERPINF1
CTSD
SERPINB3
MMP13
PLOD2
ITIH1
ITIH3
HTRA1
MMP9
ELANE
PLOD1
SERPINB12
ADAM19
SERPING1
TIMP3
SERPINA5
C1QTNF5
TGM3
SERPINF2
SEMA3B
GPC4
CSTB
F2
CTSB
PLG
CTSL
LGALS8
CTSH
LGALS7
CTSZ
HRG
KNG1
CSTA
TGM1
FCN2
PLXNB2
TIMP1
TGM2
F13A1
CST3
SERPINE2
ADAM15
ITIH5
REG1B
MUC1
SDC2
SERPINB1
FAM20B
AGT
ANXA6
LGALS2
SERPINC1
SERPINA4
ADAM17
PRSS2
SERPINH1
FCN1
LGALS1
SERPINI2
ANXA5
ANXA7
ST14
CPN2
KCP
FGL2
HPX
FREM1
ADAM9
AGRN
LAMA4
CSPG4
SDC1
PXDN
AEBP1
C1QB
ANXA2
SFTPD
EMCN
COL6A6
LMAN1
PLXNB1
SEMA4D
LGALS3
CLEC5A
LTBP4
CRIM1
LAMB2
MGP
C1QC
COL6A2
EFEMP1
LAMA3
FBLN5
COLEC10
PLXDC2
FREM2
COL15A1
DPT
PAPLN
ANXA11
ANXA4
ANXA1
MATN2
PLXND1
COL10A1
LAMA2
ECM1
SEMA3G
COL4A5
COL4A3
IGFBP7
IGFALS
MUC20
CLEC18B
COL6A1
COL8A1
COL1A2
COL5A1
FBN1
MFAP1
TINAGL1
COL18A1
COL1A1
FGG
ELN
NID1
FGB
COL12A1
COL9A2
LAMA5
MFGE8
FBN2
WISP2
NPNT
COL2A1
LAMB1
LAMC1
COL5A3
COL5A2
LAMA1
THBS1
FGA
EMILIN1
COL4A1
SPARC
SBSPON
LRG1
COL4A6
COL11A1
COL8A2
FN1
HRNR
CXCL14
COL16A1
COL4A2
COL22A1
COL3A1
LTBP1
TNC
VWA1
NTN3
COL6A3
LAMC3
CRNN
COL11A2
COL7A1
MFAP2
VWF
VTN
FNDC1
FLG
CXCL12
COL14A1
COL4A4
MFAP4
NID2
FBLN1
GDF15
S100A10
TGFBI
FGL1
S100A9
TINAG
LAMB4
ANGPTL6
S100A6
FLG2
COL21A1
S100A8
CRELD1
NTN4
THSD4
S100A14
CCBE1
MMRN2
S100A16
MFAP5
EMILIN2
S100A13
INHBC
POSTN
S100A11
OGN
PRG3
COCH
TNXB
S100A7A
EGF
INHBE
SLIT1
ACAN
ASPN
FRAS1
FGF2
EBI3
PRG2
BGN
HSPG2
PRELP
LUM
VCAN
DCN

a

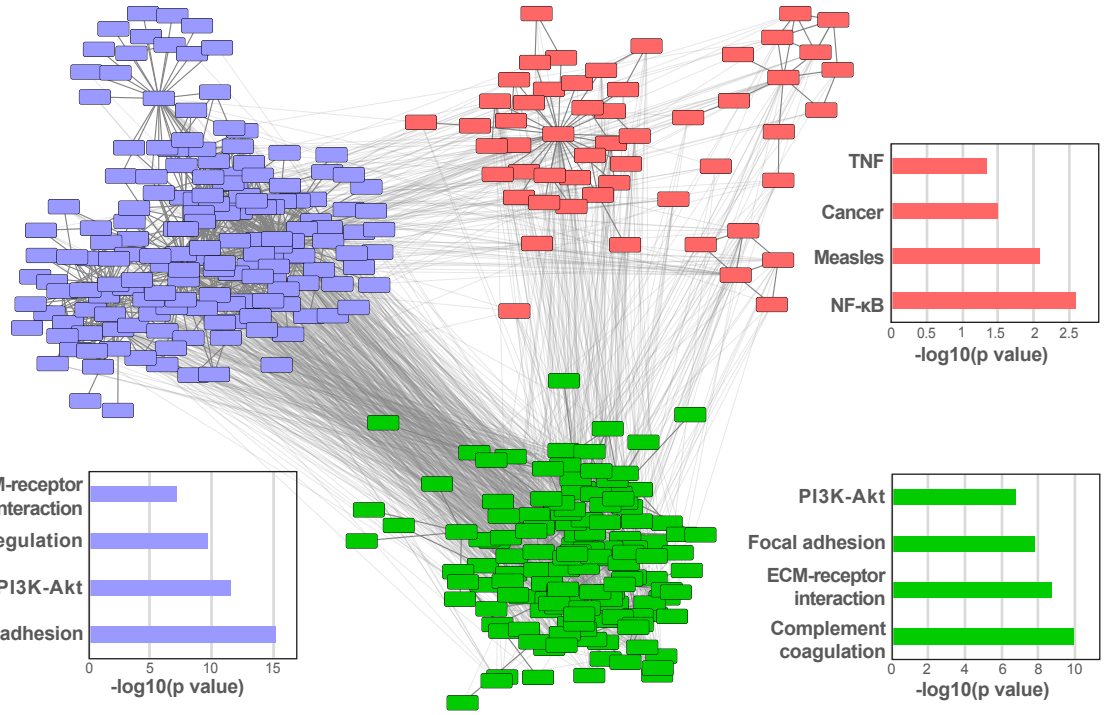
TNF
Cancer
Measles
NF-κB
0 0.5 1 1.5 2 2.5
-log10(p value)
ECM-receptor interaction
Actin regulation
PI3K-Akt
Focal adhesion
0 5 10 15
-log10(p value)
PI3K-Akt
Focal adhesion
ECM-receptor interaction
Complement coagulation
0 2 4 6 8 10
-log10(p value)

Journal of the American Society of NEPHROLOGY

Identification of an altered matrix signature in kidney ageing and disease

JASN
JOURNAL OF THE AMERICAN SOCIETY OF NEPHROLOGY

METHODS

Young & aged kidneys from mouse models & human nephrectomies

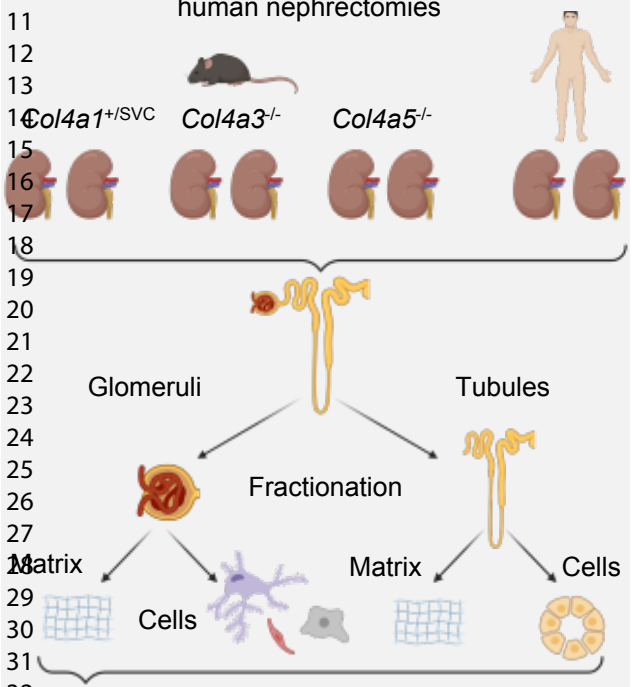

Global proteomics, ultrastructural analysis & comparison to human disease datasets

OUTCOME

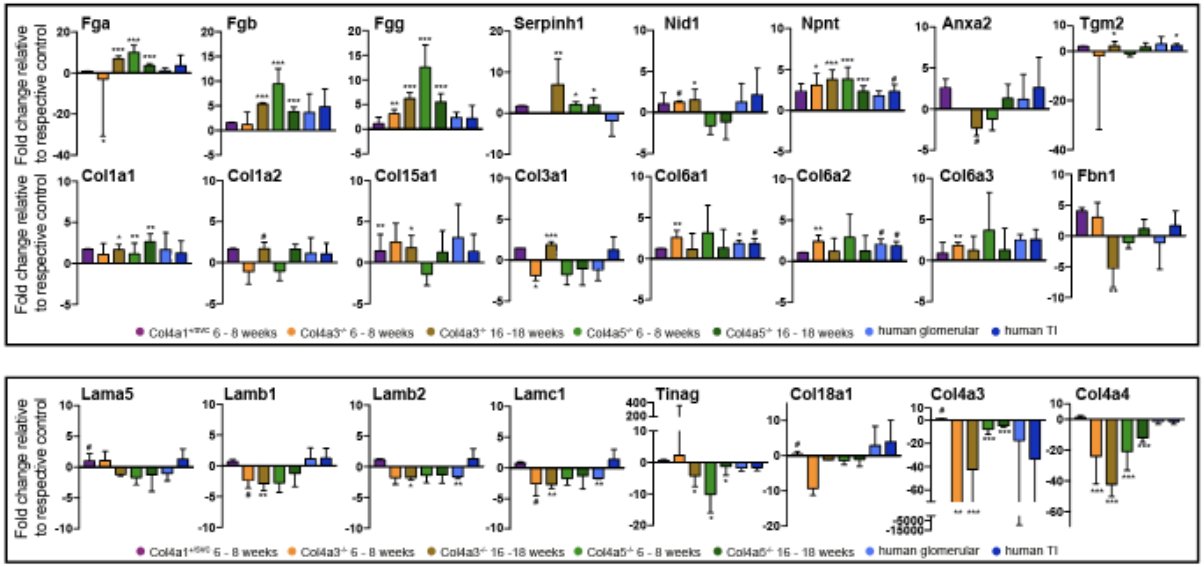

We found: 1) ultrastructural change in matrix coupled with altered matrix and cell adhesion in models of glomerular disease, 2) similar patterns of altered glomerular matrix in human ageing with a reduction in basement membrane proteins and an increase in interstitial matrix, 3) we defined the human tubulointerstitial matrisome and identified a distinct pattern of altered matrix in ageing.

Conclusion: We describe a molecular basis for altered matrix in the kidney with a reduction of basement membrane components and an increase in interstitial matrix across both ageing and disease suggesting shared pathobiology.

doi: 10.1681/ASN.